

---

# Differentiable Annealed Importance Sampling and the Perils of Gradient Noise

---

Guodong Zhang<sup>1,2</sup>, Kyle Hsu<sup>3</sup>, Jianing Li<sup>1</sup>, Chelsea Finn<sup>3</sup>, Roger Grosse<sup>1,2</sup>  
<sup>1</sup>University of Toronto, <sup>2</sup>Vector Institute, <sup>3</sup>Stanford University  
{gdzhang, rgrosse}@cs.toronto.edu  
{kylehsu, cbfinn}@cs.stanford.edu, jrobert.li@mail.utoronto.ca

## Abstract

Annealed importance sampling (AIS) and related algorithms are highly effective tools for marginal likelihood estimation, but are not fully differentiable due to the use of Metropolis-Hastings (MH) correction steps. Differentiability is a desirable property as it would admit the possibility of optimizing marginal likelihood as an objective using gradient-based methods. To this end, we propose a differentiable AIS algorithm by abandoning MH steps, which further unlocks mini-batch computation. We provide a detailed convergence analysis for Bayesian linear regression which goes beyond previous analyses by explicitly accounting for non-perfect transitions. Using this analysis, we prove that our algorithm is consistent in the full-batch setting and provide a sublinear convergence rate. However, we show that the algorithm is inconsistent when mini-batch gradients are used due to a fundamental incompatibility between the goals of last-iterate convergence to the posterior and elimination of the pathwise stochastic error. This result is in stark contrast to our experience with stochastic optimization and stochastic gradient Langevin dynamics, where the effects of gradient noise can be washed out by taking more steps of a smaller size. Our negative result relies crucially on our explicit consideration of convergence to the stationary distribution, and it helps explain the difficulty of developing practically effective AIS-like algorithms that exploit mini-batch gradients.

## 1 Introduction

Marginal likelihood (ML), sometimes called *evidence*, is a central quantity in Bayesian learning as it measures how well a model can describe a particular data set. It is commonly used to select hyperparameters for Gaussian processes [Rasmussen, 2003], where either closed-form solutions or accurate, tractable approximations are available. However, it is more often the case that computing ML is computationally intractable, as it involves summation or integration over high-dimensional model parameters or latent variables. In this case, one must resort to numerical approximation methods. In the context of model comparison (e.g., evaluating generative models [Wu et al., 2016, Huang et al., 2020]), annealed importance sampling (AIS) [Neal, 2001] is arguably the most popular algorithm. Notably, AIS is closely related to other generic ML estimators that yield accurate estimation [Grosse et al., 2015], including Sequential Monte Carlo (SMC) [Doucet et al., 2001] and nested sampling [Skilling et al., 2006]. Given enough computing time, AIS is able to produce accurate estimates of marginal likelihood (it converges to the true ML value quickly by adding more intermediate distributions).

AIS alternates between Markov chain Monte Carlo (MCMC) transitions and importance sampling updates, where the MCMC step typically involves a non-differentiable Metropolis-Hastings (MH) correction. Unfortunately, the MH step is generally incompatible with gradient-based optimization and complicates theoretical analysis. To resolve these issues, we marry AIS with Hamiltonian Monte

Carlo (HMC) [Neal et al., 2011] and derive an unbiased yet differentiable ML estimator named differentiable AIS (DAIS) by removing the MH correction step, which further unlocks the possibility of mini-batch computation. Moreover, our algorithm can be made memory-efficient by caching noise and simulating Hamiltonian dynamics in reverse [Maclaurin et al., 2015]. We further prove that DAIS is asymptotically consistent with full-batch gradients in the case of Bayesian linear regression, inheriting the convergence property of AIS. In particular, we provide a sublinear convergence rate by explicitly accounting for non-perfect transitions<sup>1</sup>.

Furthermore, motivated by the problem of learning from large-scale datasets, we study a stochastic variant of our algorithm that uses gradients estimated from a subset of the dataset. Given the success of stochastic optimization [Robbins and Monro, 1951] and stochastic gradient MCMC algorithms [Welling and Teh, 2011, Chen et al., 2014], one may presume that stochastic gradient DAIS performs well. Surprisingly, the natural implementation of this algorithm can be arbitrarily bad. In particular, we show that DAIS with stochastic gradients is inconsistent due to a fundamental incompatibility between the goals of last-iterate convergence to the posterior and elimination of the pathwise stochastic error. This is in stark contrast with other settings such as gradient-based optimization and Langevin dynamics, where the gradient noise can be washed out by taking smaller steps. This indicates that ML estimation with stochastic gradients may require new ideas.

We validate our theoretical analysis with simulations. We also demonstrate empirically that DAIS can be applied to variational autoencoders (VAEs) [Kingma and Welling, 2013] for a tighter evidence lower bound, which in turn leads to improved performance compared to vanilla VAE. We also compare to importance weighted autoencoders (IWAE) [Burda et al., 2016]. While IWAE is more effective with a low compute budget, we show that DAIS eventually outperforms IWAE as compute increases. Finally, like AIS, DAIS can be used to evaluating generative models. We show that it performs on par with AIS despite the removal of the MH correction step and outperforms the IWAE bound by a large margin.

## 2 Background

### 2.1 Marginal Likelihood Estimation

For a model  $\mathcal{M}$  and observed data  $\mathcal{D}$ , one can define marginal likelihood (ML) as

$$p(\mathcal{D}|\mathcal{M}) = \int p(\mathcal{D}, \boldsymbol{\theta}|\mathcal{M})d\boldsymbol{\theta} = \int p(\mathcal{D}|\boldsymbol{\theta}, \mathcal{M})p(\boldsymbol{\theta}|\mathcal{M})d\boldsymbol{\theta}, \quad (1)$$

where  $\boldsymbol{\theta}$  denotes the parameters of the model. ML estimation is often regarded as the same problem as estimating the partition function of an unnormalized distribution. Given a distribution defined as  $p(\boldsymbol{\theta}) = f(\boldsymbol{\theta})/\mathcal{Z}$  where the unnormalized density  $f(\boldsymbol{\theta})$  can be efficiently computed, we are interested in estimating the partition function  $\mathcal{Z} = \int f(\boldsymbol{\theta})d\boldsymbol{\theta}$ . In (1), the  $f(\boldsymbol{\theta})$  is  $p(\mathcal{D}, \boldsymbol{\theta}|\mathcal{M})$ . In this paper, we find it convenient to focus on discussing ML estimation because we later will discuss the effect of noise arising from data subsampling.

It is often the case that computing ML is computationally intractable. One approach is to approximate (1) with Monte Carlo methods. In particular, one can approximate the integration using importance sampling:

$$p(\mathcal{D}|\mathcal{M}) = \mathbb{E}_{q(\boldsymbol{\theta})} \left[ \frac{p(\mathcal{D}|\boldsymbol{\theta}, \mathcal{M})p(\boldsymbol{\theta}|\mathcal{M})}{q(\boldsymbol{\theta})} \right] \approx \frac{1}{S} \sum_{i=1}^S \frac{p(\mathcal{D}|\boldsymbol{\theta}_i, \mathcal{M})p(\boldsymbol{\theta}_i|\mathcal{M})}{q(\boldsymbol{\theta}_i)} \quad \text{with } \boldsymbol{\theta}_i \sim q(\boldsymbol{\theta}) \quad (2)$$

However, this estimation can exhibit high variance for small or medium  $S$  when the target distribution  $p(\mathcal{D}, \boldsymbol{\theta}|\mathcal{M})$  and proposal distribution  $q(\boldsymbol{\theta})$  are dissimilar.

### 2.2 Annealed Importance Sampling

Annealed importance sampling (AIS) is an algorithm which estimates the ML by gradually changing, or “annealing”, a distribution. Formally, the algorithm takes in a sequence of distributions  $p_0, \dots, p_K$ ,

<sup>1</sup>While Neal [2001] analyzed the convergence rate of AIS, his analysis assumed perfect transitions. In this paper, we show that accounting for the convergence of concrete MCMC algorithms is crucial for understanding the practical performance.

with  $p_k(\boldsymbol{\theta}) = f_k(\boldsymbol{\theta})/\mathcal{Z}_k$  and  $\mathcal{Z}_k = \int f_k(\boldsymbol{\theta})d\boldsymbol{\theta}$ . In the context of ML estimation, the starting distribution  $f_0$  is the tractable prior distribution  $p(\boldsymbol{\theta}|\mathcal{M})$  with  $\mathcal{Z}_0 = 1$ , while the target distribution  $f_K$  is  $p(\mathcal{D}, \boldsymbol{\theta}|\mathcal{M})$  with  $\mathcal{Z}_K = p(\mathcal{D}|\mathcal{M})$ . For each  $p_k$ , one must also specify an MCMC transition operator  $\mathcal{T}_k$  which leaves  $p_k$  invariant.

The output of AIS is an unbiased estimate  $\hat{\mathcal{Z}}_K$  of the exact ML  $\mathcal{Z}_K$ . Importantly, unbiasedness holds for any finite  $K$ , as shown in Neal [2001]. Moreover, AIS can be viewed as importance sampling over an extended space [Neal, 2001]. In particular, we have  $\mathcal{Z}_K = \mathbb{E}_{q_{\text{fwd}}} [q_{\text{bwd}}/q_{\text{fwd}}]$  with the target and proposal distributions defined as

$$q_{\text{fwd}}(\boldsymbol{\theta}_{0:K}) = p_0(\boldsymbol{\theta}_0)\mathcal{T}_1(\boldsymbol{\theta}_1|\boldsymbol{\theta}_0) \cdots \mathcal{T}_K(\boldsymbol{\theta}_K|\boldsymbol{\theta}_{K-1}) \quad (3)$$

$$q_{\text{bwd}}(\boldsymbol{\theta}_{0:K}) = f_K(\boldsymbol{\theta}_K)\tilde{\mathcal{T}}_K(\boldsymbol{\theta}_{K-1}|\boldsymbol{\theta}_K) \cdots \tilde{\mathcal{T}}_1(\boldsymbol{\theta}_0|\boldsymbol{\theta}_1), \quad (4)$$

where  $\mathcal{T}_k(\boldsymbol{\theta}|\boldsymbol{\theta}')$  is a forward MCMC kernel and  $\tilde{\mathcal{T}}_k(\boldsymbol{\theta}'|\boldsymbol{\theta}) = \mathcal{T}_k(\boldsymbol{\theta}|\boldsymbol{\theta}')p_k(\boldsymbol{\theta}')/p_k(\boldsymbol{\theta})$  is the corresponding reverse MCMC kernel. Here,  $q_{\text{fwd}}$  represents the chain of states generated by AIS, and  $q_{\text{bwd}}$  is a fictitious (unnormalized) reverse chain which begins with a sample from  $p_K$  and applies the transitions in reverse order. In practice, the intermediate distributions have to be chosen carefully for a low variance estimate  $\hat{\mathcal{Z}}_K$ . One typically uses geometric averages of the initial and target distributions:

$$p_k(\boldsymbol{\theta}) = p_{\beta_k}(\boldsymbol{\theta}) = f_{\beta_k}(\boldsymbol{\theta})/\mathcal{Z}_{\beta_k} = f_0(\boldsymbol{\theta})^{1-\beta_k} f_K(\boldsymbol{\theta})^{\beta_k} / \mathcal{Z}_{\beta_k} = p(\boldsymbol{\theta}|\mathcal{M})p(\mathcal{D}|\boldsymbol{\theta}, \mathcal{M})^{\beta_k} / \mathcal{Z}_{\beta_k} \quad (5)$$

where  $0 = \beta_0 < \beta_1 < \cdots < \beta_K = 1$  is the annealing schedule. Indeed, AIS gives an unbiased estimate  $\hat{\mathcal{Z}}$  of  $\mathcal{Z}$ . However, as  $\mathcal{Z}$  can vary over many orders of magnitude, it is often more meaningful to talk about estimating  $\log \mathcal{Z}$ . Unfortunately, unbiased estimators of  $\mathcal{Z}$  can result in biased estimators of  $\log \mathcal{Z}$  because  $\mathbb{E} \log \hat{\mathcal{Z}} \leq \log \mathbb{E} \hat{\mathcal{Z}}$  by Jensen's inequality, resulting in only a lower bound. In particular, we have the AIS bound

$$\mathbb{E}_{q_{\text{fwd}}} \log \hat{\mathcal{Z}}_K = \sum_{k=1}^K \mathbb{E}_{q_{\text{fwd}}} [\log f_{\beta_k}(\boldsymbol{\theta}_{k-1}) - \log f_{\beta_{k-1}}(\boldsymbol{\theta}_{k-1})] \quad (6)$$

$$= \sum_{k=1}^K (\beta_k - \beta_{k-1}) \mathbb{E}_{q_{\text{fwd}}} [\log p(\mathcal{D}|\boldsymbol{\theta}_{k-1}, \mathcal{M})] \quad (7)$$

where (5) facilitated the simplification from (6) to (7). Of course, it is not enough to have a lower bound; we would also like the estimates to be close to the true value. Fortunately, AIS is *consistent* in that it converges to the correct value in the limit of infinite intermediate distributions[Neal, 2001].

### 3 Differentiable Annealed Importance Sampling

In this section, we motivate and derive a differentiable AIS (DAIS) algorithm for ML estimation. We also discuss its application to variational inference and a memory-efficient implementation.

Ideally, assuming a continuously parameterized model class (e.g., variational autoencoder), we would like to differentiate through the lower bound (7) to find an optimal model  $\mathcal{M}$ . However, AIS must be instantiated with an MCMC transition kernel  $\mathcal{T}_k$  that satisfies detailed balance to ensure it leaves  $p_k$  invariant. In practice, this is typically achieved by using a MH step, which is generally not differentiable.<sup>2</sup> We thus

remove the MH correction and, in particular, specify each transition to consist of a deterministic leapfrog integration step followed by a stochastic partial momentum refreshment [Horowitz, 1991]. Algorithm 1 details the simulation of Hamiltonian dynamics using such transitions. With  $\gamma = 0$ , the

---

#### Algorithm 1 Differentiable AIS (DAIS)

---

$\boldsymbol{\theta}_0, \mathbf{v}_0$  sample from  $p_0(\boldsymbol{\theta}), \pi \triangleq \mathcal{N}(\mathbf{0}, \mathbf{M})$   
 $\mathcal{L}_{\text{DAIS}} = -\log p_0(\boldsymbol{\theta}_0)$   
**for**  $k = 1, \dots, K$  **do**  
 $\boldsymbol{\theta}_{k-\frac{1}{2}} \leftarrow \boldsymbol{\theta}_{k-1} + \frac{\eta}{2} \mathbf{M}^{-1} \mathbf{v}_{k-1}$   
 $\hat{\mathbf{v}}_k \leftarrow \mathbf{v}_{k-1} + \eta \nabla \log f_{\beta_k}(\boldsymbol{\theta}_{k-\frac{1}{2}})$   
 $\boldsymbol{\theta}_k \leftarrow \boldsymbol{\theta}_{k-\frac{1}{2}} + \frac{\eta}{2} \mathbf{M}^{-1} \hat{\mathbf{v}}_k$   
 $\mathbf{v}_k \leftarrow \gamma \hat{\mathbf{v}}_k + \sqrt{1-\gamma^2} \boldsymbol{\varepsilon}, \boldsymbol{\varepsilon} \sim \mathcal{N}(\mathbf{0}, \mathbf{M})$   
 $\mathcal{L}_{\text{DAIS}} += \log \pi(\hat{\mathbf{v}}_k) - \log \pi(\mathbf{v}_{k-1})$   
**end for**  
**return**  $\mathcal{L}_{\text{DAIS}} += \log p(\mathcal{D}, \boldsymbol{\theta}_K|\mathcal{M})$

---

<sup>2</sup>The discontinuity introduced by the MH step makes it hard to use the reparameterization trick, though this can be done using a delicate gradient estimator [Naesseth et al., 2017]. This is orthogonal to our work and our fix is simpler and easier for us to analyze.

algorithm is essentially unadjusted Langevin dynamics [Roberts et al., 1996]. In practice, choosing  $0 < \gamma < 1$  ( $\gamma = 0.9$  is a common default) helps avoid random walk behavior and accelerates mixing [Neal et al., 2011, Chen et al., 2014]. Importantly, we retain the formalism of performing importance sampling on an extended space despite the loss of detailed balance. To show this, we can define the forward and (unnormalized) backward distributions as

$$q_{\text{fwd}}(\boldsymbol{\theta}_{0:K}, \mathbf{v}_{0:K}) = p_0(\boldsymbol{\theta}_0)\pi(\mathbf{v}_0)\mathcal{T}_1(\boldsymbol{\theta}_1, \mathbf{v}_1|\boldsymbol{\theta}_0, \mathbf{v}_0) \cdots \mathcal{T}_K(\boldsymbol{\theta}_K, \mathbf{v}_K|\boldsymbol{\theta}_{K-1}, \mathbf{v}_{K-1}) \quad (8)$$

$$q_{\text{bwd}}(\boldsymbol{\theta}_{0:K}, \mathbf{v}_{0:K}) = f_K(\boldsymbol{\theta}_K)\pi(\mathbf{v}_K)\tilde{\mathcal{T}}_K(\boldsymbol{\theta}_{K-1}, \mathbf{v}_{K-1}|\boldsymbol{\theta}_K, \mathbf{v}_K) \cdots \tilde{\mathcal{T}}_1(\boldsymbol{\theta}_0, \mathbf{v}_0|\boldsymbol{\theta}_1, \mathbf{v}_1) \quad (9)$$

where the transition operator  $\mathcal{T}_k(\boldsymbol{\theta}_k, \mathbf{v}_k|\boldsymbol{\theta}_{k-1}, \mathbf{v}_{k-1}) = \mathcal{T}'_k(\boldsymbol{\theta}_k, \hat{\mathbf{v}}_k|\boldsymbol{\theta}_{k-1}, \mathbf{v}_{k-1})\mathcal{T}''_k(\mathbf{v}_k|\hat{\mathbf{v}}_k)$  is the composition of a leapfrog step and momentum refreshment step. We define the reverse chain by starting with an exact sample and executing each of the above steps of Algorithm 1 in the reverse order, which leads to a surprisingly simple expression for our estimator. In particular, the backward transition operator is defined by  $\tilde{\mathcal{T}}_k(\boldsymbol{\theta}_{k-1}, \mathbf{v}_{k-1}|\boldsymbol{\theta}_k, \mathbf{v}_k) = \mathcal{T}''_k(\hat{\mathbf{v}}_k|\mathbf{v}_k)\mathcal{T}'_k(\boldsymbol{\theta}_{k-1}, \mathbf{v}_{k-1}|\boldsymbol{\theta}_k, -\hat{\mathbf{v}}_k)$ . Note that we need to flip the sign of  $\hat{\mathbf{v}}_k$  in the reverse chain to account for time reversal. As a consequence of the above definitions, we have

$$\mathcal{T}''_k(\mathbf{v}_k|\hat{\mathbf{v}}_k) = \mathcal{T}''_k(\hat{\mathbf{v}}_k|\mathbf{v}_k)\pi(\mathbf{v}_k)/\pi(\hat{\mathbf{v}}_k). \quad (10)$$

This is because  $\mathcal{T}''_k(\mathbf{v}_k|\hat{\mathbf{v}}_k) = \mathcal{N}(\gamma\hat{\mathbf{v}}_k, (1-\gamma^2)\mathbf{M})$  and  $\mathcal{T}''_k(\hat{\mathbf{v}}_k|\mathbf{v}_k) = \mathcal{N}(\gamma\mathbf{v}_k, (1-\gamma^2)\mathbf{M})$ . Furthermore, since  $\mathcal{T}'_k$  is a deterministic leapfrog update, it is reversible and volume preserving, so we have  $\mathcal{T}'_k(\boldsymbol{\theta}_{k-1}, \mathbf{v}_{k-1}|\boldsymbol{\theta}_k, -\hat{\mathbf{v}}_k) = \mathcal{T}'_k(\boldsymbol{\theta}_k, \hat{\mathbf{v}}_k|\boldsymbol{\theta}_{k-1}, \mathbf{v}_{k-1})$ . With this, we can derive the DAIS bound:

$$\begin{aligned} \mathcal{L}_{\text{DAIS}} &= \mathbb{E}_{q_{\text{fwd}}} [\log q_{\text{bwd}}(\boldsymbol{\theta}_{0:K}, \mathbf{v}_{0:K}) - \log q_{\text{fwd}}(\boldsymbol{\theta}_{0:K}, \mathbf{v}_{0:K})] \\ &= \mathbb{E}_{q_{\text{fwd}}} \left[ \log p(\mathcal{D}, \boldsymbol{\theta}_K|\mathcal{M}) - \log p_0(\boldsymbol{\theta}_0) + \sum_{k=1}^K \log \frac{\pi(\hat{\mathbf{v}}_k)}{\pi(\mathbf{v}_{k-1})} \right] \end{aligned} \quad (11)$$

We remark that this bound supports the computation of pathwise derivatives.

It's useful to consider an intuition for the final term of (11), since this will help to clarify our convergence analysis. Observe that  $\log \pi(\mathbf{v}_k)$  is simply the negative kinetic energy plus a constant, so this term will be negative if the kinetic energy increases over the course of a leapfrog step and positive if it decreases. For small enough step sizes, leapfrog steps approximately conserve the total energy. If the posterior distribution is becoming more concentrated over the course of annealing (as is typically the case), the start of the leapfrog step is likely to have atypically high potential energy, so the leapfrog step will convert the potential energy to kinetic energy, and this term will be negative in expectation. Conversely, if the distribution is becoming more spread out, kinetic energy will be converted to potential energy, and the term will be positive in expectation. Hence, when summed over the whole trajectory, this term helps to estimate the volume of the support of the posterior distribution.

### 3.1 Differentiable Annealed Variational Inference

DAIS can be applied to variational inference for a tighter bound; we name this differentiable annealed variational inference (DAVI). We note that the general idea of incorporating auxiliary MCMC states into a variational approximation was discussed in Salimans et al. [2015], but their formulation requires the specification and learning of a reverse transition model, whereas ours does not.

Recall that we can lower bound the log ML by choosing a tractable variational distribution and optimizing the bound. This has been widely adopted in variational autoencoders [Kingma and Welling, 2013, Rezende et al., 2014] and Bayesian neural networks [Blundell et al., 2015, Zhang et al., 2018]. The lower bound has the following form:

$$\mathcal{L} \equiv \mathbb{E}_{q_\phi} [\log p(\mathcal{D}, \boldsymbol{\theta}|\mathcal{M}) - \log q_\phi(\boldsymbol{\theta})] \quad (12)$$

However, the lower bound can be quite loose if the variational posterior family  $q_\phi(\boldsymbol{\theta})$  is restrictive, e.g. Gaussian. To improve the bound, we can define a new variational distribution on an extended space as in (8), but starting from  $q_\phi$  rather than  $p_0$ :

$$q_{\text{fwd}}(\boldsymbol{\theta}_{0:K}, \mathbf{v}_{0:K}) = q_\phi(\boldsymbol{\theta}_0)\pi(\mathbf{v}_0)\mathcal{T}_1(\boldsymbol{\theta}_1, \mathbf{v}_1|\boldsymbol{\theta}_0, \mathbf{v}_0) \cdots \mathcal{T}_K(\boldsymbol{\theta}_K, \mathbf{v}_K|\boldsymbol{\theta}_{K-1}, \mathbf{v}_{K-1}). \quad (13)$$

We also define associated intermediate distributions  $p_k(\boldsymbol{\theta}) = q_\phi(\boldsymbol{\theta})^{1-\beta_k}p(\mathcal{D}, \boldsymbol{\theta}|\mathcal{M})^{\beta_k}$ . This gives a new lower bound:

$$\mathcal{L}_{\text{DAVI}} \equiv \mathbb{E}_{q_{\text{fwd}}} \left[ \log p(\mathcal{D}, \boldsymbol{\theta}_K|\mathcal{M}) - \log q_\phi(\boldsymbol{\theta}_0) + \sum_{k=1}^K \log \frac{\pi(\hat{\mathbf{v}}_k)}{\pi(\mathbf{v}_{k-1})} \right]. \quad (14)$$

We can maximize this lower bound over model parameters of  $\mathcal{M}$ , all parameters of AIS (e.g., annealing schedule  $\beta_k$ ) as well as variational parameters  $\phi$ .

### 3.2 Memory-Efficient Implementation

Naively optimizing instantiations of (11) or (14) w.r.t. parameters using reverse-mode differentiation involves storing the entire sequence of sampled states  $\theta_0, \mathbf{v}_0, \dots, \theta_K, \mathbf{v}_K$ . This can be problematic in cases when  $K$  is large due to the large memory overhead. However, DAIS is compatible with the idea of reversible learning [Maclaurin et al., 2015], which ameliorates this problem. Instead of storing the states in memory, we can compute the previous state given the current state by reversing the dynamics. Recall that each DAIS transition is deterministic and reversible other than the use of noise  $\varepsilon_k$  for momentum refreshment. The exact noise samples can also be computed in reverse if one uses a deterministic and reversible scheme (e.g. the linear congruential generator) for managing pseudorandom number generator seeds. Assuming exact arithmetic (in practice, this is impossible), this means that the memory footprint of DAIS can be made *constant* with respect to the number of intermediate distributions  $K$ . Similar memory-efficiency tricks have also been used in other applications [Li et al., 2020, Ruan et al., 2021].

However, as discussed by Maclaurin et al. [2015], reversible learning with finite arithmetic precision requires some storage to counteract compounding round-off error. For  $\gamma \neq 0$  ( $\gamma = 0.9$  is a common default), we need on average  $\log_2(1/\gamma)$  bits per parameter per step, which is still small compared to naive storage. We defer further exposition on memory-efficient DAIS to Appendix D. We remark that reversible learning is a potentially crucial property of DAIS as it affords some degree of scaling to longer chain lengths and, indirectly, bigger models.

## 4 Convergence Analysis for Bayesian Linear Regression

Neal [2001] and others have pointed that AIS is consistent, i.e. that it converges to the true log-ML value in the limit of infinite intermediate distributions. However, these existing consistency results largely depend on the assumption that each transition  $\mathcal{T}_k$  generates a state from  $p_k$ , independent of the previous state. This is unrealistic in practice.

Here, we analyze DAIS without the assumption of perfect transitions. In particular, we focus on the Bayesian linear regression setting and adopt the following model:

$$\text{prior: } \theta \sim \mathcal{N}(\mu_p, \Lambda_p^{-1})$$

$$\text{likelihood: } \theta \sim \mathcal{N}(\mu_*, \Lambda_{\text{lld}}^{-1}) \text{ where } \Lambda_{\text{lld}} = \sigma^{-2} \mathbf{X}^\top \mathbf{X} \text{ and } \mu_* = (\mathbf{X}^\top \mathbf{X})^{-1} \mathbf{X}^\top \mathbf{y}$$

$$\text{posterior: } \theta \sim \mathcal{N}(\mu_{\text{pos}}, \Lambda_{\text{pos}}^{-1}) \text{ where } \mu_{\text{pos}} = \Lambda_{\text{pos}}^{-1} (\Lambda_p \mu_p + \Lambda_{\text{lld}} \mu_*) \text{ and } \Lambda_{\text{pos}} = \Lambda_p + \Lambda_{\text{lld}}$$

with  $\mathbf{X} \in \mathbb{R}^{n \times d}$  denoting the input features and  $\mathbf{y} \in \mathbb{R}^{n \times 1}$  the targets. We choose Bayesian linear regression because it enables us to analyze the dynamics analytically in a similar manner as done by the noisy quadratic model (NQM) [Zhang et al., 2019] in the context of optimization. We adopt the leapfrog step (we assume an identity mass matrix without loss of generality because we can absorb  $\mathbf{M}$  into the input matrix  $\mathbf{X}$  in Algorithm 1) and obtain the following update rule (see Appendix B.1 for derivation):

$$\begin{aligned} \theta_k &\leftarrow \left( \mathbf{I} - \frac{\eta_k^2}{2} \Lambda_{\text{pos}}^{\beta_k} \right) \theta_{k-1} + \left( \eta_k \mathbf{I} - \frac{\eta_k^3}{4} \Lambda_{\text{pos}}^{\beta_k} \right) \mathbf{v}_{k-1} + \frac{\eta_k^2}{2} \Lambda_{\text{pos}}^{\beta_k} \mu_{\text{pos}}^{\beta_k} \\ \hat{\mathbf{v}}_k &\leftarrow -\eta_k \Lambda_{\text{pos}}^{\beta_k} \theta_{k-1} + \left( \mathbf{I} - \frac{\eta_k^2}{2} \Lambda_{\text{pos}}^{\beta_k} \right) \mathbf{v}_{k-1} + \eta_k \Lambda_{\text{pos}}^{\beta_k} \mu_{\text{pos}}^{\beta_k} \end{aligned} \quad (15)$$

where  $\Lambda_{\text{pos}}^{\beta_k} = \Lambda_p + \beta_k \Lambda_{\text{lld}}$  and  $\mu_{\text{pos}}^{\beta_k} = (\Lambda_{\text{pos}}^{\beta_k})^{-1} (\Lambda_p \mu_p + \beta_k \Lambda_{\text{lld}} \mu_*)$ . With these iterative updates, we can compute the expectation and covariance of  $\theta_k$  and  $\mathbf{v}_k$  at any time  $k$ , which suffices to compute the lower bound in closed-form.

**Table 1:** Memory and time usage of DAIS implementations.  $B$  is 32 for single-precision floating-point format.

Scheme	Precision	Memory	Time
Naive	finite	$\mathcal{O}(BK)$	$\mathcal{O}(K)$
Rev. Learning	finite	$\mathcal{O}(\log_2(1/\gamma)K)$	$\mathcal{O}(K)$

#### 4.1 Sublinear Convergence in the Full-Batch Setting

With the model defined, we now show that our algorithm is asymptotically consistent, i.e., the bound (11) converges to exact log ML as  $K$  goes to infinity. For Bayesian linear regression, the update rules in (15) are affine transformations of Gaussian random variables, so the distribution of  $\theta_k$  is also Gaussian in the form of  $\mathcal{N}(\boldsymbol{\mu}_k, \boldsymbol{\Sigma}_k)$ . We can compute the gap between the log ML and our lower bound in closed-form (see Appendix B.2 for derivation):

$$\log p(\mathcal{D}) - \mathcal{L}_{\text{DAIS}} = \underbrace{\frac{1}{2} \|\boldsymbol{\mu}_K - \boldsymbol{\mu}_{\text{pos}}\|_{\boldsymbol{\Lambda}_{\text{pos}}}^2}_{\textcircled{1}} + \underbrace{\frac{1}{2} \text{Tr}(\boldsymbol{\Lambda}_{\text{pos}} \boldsymbol{\Sigma}_K) - \frac{d}{2}}_{\textcircled{2}} + \underbrace{\frac{1}{2} \log \frac{|\boldsymbol{\Sigma}_{\text{pos}}|}{|\boldsymbol{\Sigma}_p|} - \mathbb{E}_q \left[ \sum_{k=1}^K \log \frac{\pi(\hat{\mathbf{v}}_k)}{\pi(\mathbf{v}_{k-1})} \right]}_{\textcircled{3}} \quad (16)$$

where  $d$  is the feature dimension. Here,  $\textcircled{1}$  and  $\textcircled{2}$  measure the error of last-iterate Markov chain convergence and will both vanish as long as  $\boldsymbol{\mu}_K \rightarrow \boldsymbol{\mu}_{\text{pos}}$  and  $\boldsymbol{\Sigma}_K \rightarrow \boldsymbol{\Sigma}_{\text{pos}}$ . We will show later that they converge with a rate of  $\mathcal{O}(\frac{1}{\eta^2 K})$ . The key is to show that  $\boldsymbol{\mu}_k$  (resp.  $\boldsymbol{\Lambda}_k$ ) lags behind  $\boldsymbol{\mu}_{\text{pos}}^{\beta_k}$  (resp.  $\boldsymbol{\Lambda}_{\text{pos}}^{\beta_k}$ ) with roughly  $\frac{1}{\eta^2}$  steps. Formally, we have the following.

**Lemma 1.** *Given equally spaced  $\beta_k$ , running DAIS with  $\gamma = 0$  and  $\eta \sim \frac{1}{K^c}$  where  $c \geq \frac{1}{4}$  yields*

$$\|\boldsymbol{\mu}_{k-1} - \boldsymbol{\mu}_{\text{pos}}^{\beta_k}\|_2 = \mathcal{O}(K^{2c-1}), \quad \|\boldsymbol{\Lambda}_{k-1} - \boldsymbol{\Lambda}_{\text{pos}}^{\beta_k}\|_2 = \mathcal{O}(K^{2c-1}). \quad (17)$$

We remark that the assumption of  $\beta_k$  being equally spaced is not essential and can be relaxed as long as they are chosen by a scheme that leads to  $\beta_k - \beta_{k-1}$  going down approximately in inverse proportion to  $K$ . In addition, we note that the assumption of full momentum refreshment is for convenience and we believe a similar result holds for  $\gamma > 0$ .

Importantly, this lemma implies that both  $\textcircled{1}$  and  $\textcircled{2}$  vanish sublinearly if we choose  $c < \frac{1}{2}$ . The analysis of error term  $\textcircled{3}$  is more nuanced. In particular, this error could either come from using transitions for each of these intermediate distributions that do not bring the distribution close to equilibrium, or from using a finite number of distributions to anneal from  $p_0$  to  $p_K$ . Surprisingly, the error  $\textcircled{3}$  decays as fast as the other two terms if the step size scales as  $1/K^c$  with  $c \geq \frac{1}{4}$ . In summary, we have the following theorem.

**Theorem 1.** *Given equally spaced  $\beta_k$ , running DAIS with  $\gamma = 0$  and  $\eta \sim \frac{1}{K^c}$  where  $c \geq \frac{1}{4}$  yields*

$$\log p(\mathcal{D}) - \mathcal{L}_{\text{DAIS}} = \mathcal{O}(K^{2c-1}).$$

With  $c = \frac{1}{4}$ , we have the optimal convergence rate  $\mathcal{O}(1/\sqrt{K})$ .

We remark that with perfect transitions, the requirement of  $c \geq 1/4$  is not necessary and we can achieve  $\mathcal{O}(1/K)$  convergence, as also shown in Grosse et al. [2013]. The gap between  $\mathcal{O}(1/\sqrt{K})$  and  $\mathcal{O}(1/K)$  highlights the importance of considering convergence to the stationary distribution.

#### 4.2 Inconsistency in the Stochastic Setting

We have shown that our algorithm is asymptotically consistent in the full-batch setting. Often, a consistent/convergent algorithm in the deterministic setting readily implies a similar convergence result in the stochastic setting. For example, SGD [Robbins and Monro, 1951] and SGMCMC [Chen et al., 2014, Ma et al., 2015] are both convergent in the presence of noise. This begs the question of whether DAIS is consistent when we only have access to stochastic gradients. Here, we adopt an additive noise model<sup>3</sup>  $\nabla \log f_k(\boldsymbol{\theta}) = \nabla \log f_k(\boldsymbol{\theta}) + \boldsymbol{\varepsilon}$ . This model is commonly used in the stochastic approximation literature, and such a model has also been adopted in Welling and Teh [2011]. With such a noise model, we have the following dynamics:

$$\begin{aligned} \boldsymbol{\theta}_k &\leftarrow \left( \mathbf{I} - \frac{\eta_k^2}{2} \boldsymbol{\Lambda}_{\text{pos}}^{\beta_k} \right) \boldsymbol{\theta}_{k-1} + \left( \eta_k \mathbf{I} - \frac{\eta_k^3}{4} \boldsymbol{\Lambda}_{\text{pos}}^{\beta_k} \right) \mathbf{v}_{k-1} + \frac{\eta_k^2}{2} \boldsymbol{\Lambda}_{\text{pos}}^{\beta_k} \boldsymbol{\mu}_{\text{pos}}^{\beta_k} + \frac{\eta_k^2}{2} \boldsymbol{\varepsilon} \\ \hat{\mathbf{v}}_k &\leftarrow -\eta_k \boldsymbol{\Lambda}_{\text{pos}}^{\beta_k} \boldsymbol{\theta}_{k-1} + \left( \mathbf{I} - \frac{\eta_k^2}{2} \boldsymbol{\Lambda}_{\text{pos}}^{\beta_k} \right) \mathbf{v}_{k-1} + \eta_k \boldsymbol{\Lambda}_{\text{pos}}^{\beta_k} \boldsymbol{\mu}_{\text{pos}}^{\beta_k} + \eta_k \boldsymbol{\varepsilon} \end{aligned} \quad (18)$$

<sup>3</sup>In reality, the noise consists of two parts: multiplicative input subsampling noise and additive label noise. We can assume that the noise is lower bounded by the additive part. See Appendix B.4 for justifications.

where stochastic noise  $\varepsilon$  has variance lowered bounded by  $\Sigma_\varepsilon$ . Further, we let  $\boldsymbol{\mu}_k^y = \mathbb{E}[\hat{\mathbf{v}}_k]$  and  $\Sigma_k^y$  be the covariance of  $\hat{\mathbf{v}}_k$ . Surprisingly, we find that DAIS is incompatible with stochastic gradients, as summarized in the following theorem:

**Theorem 2.** *For stochastic DAIS with full momentum refreshment ( $\gamma = 0$  in Algorithm 1) and any stepsize scheme, we have*

$$\liminf_{K \rightarrow \infty} |\log p(\mathcal{D}) - \mathcal{L}_{DAIS}| > 0. \quad (19)$$

Here, we give some intuition why DAIS fails in the stochastic setting. To ensure convergence of  $\boldsymbol{\theta}_K$  to  $\mathcal{N}(\boldsymbol{\mu}_{\text{pos}}, \Sigma_{\text{pos}})$ , a major requirement is for the step sizes to satisfy the property [Robbins and Monro, 1951] of  $\lim_{K \rightarrow \infty} \sum_{k=1}^K \eta_k^2 = \infty$ . However, the randomness of mini-batching sampling would contribute to the variance of  $\hat{\mathbf{v}}_k$ . In particular, we have the following recursion:

$$\tilde{\Sigma}_k^y = \eta_k^2 \Lambda_{\text{pos}}^{\beta_k} \hat{\Sigma}_{k-1} \Lambda_{\text{pos}}^{\beta_k} + \left( \mathbf{I} - \frac{\eta_k^2}{2} \Lambda_{\text{pos}}^{\beta_k} \right)^2 + \eta_k^2 \Sigma_\varepsilon. \quad (20)$$

For notational convenience, we let  $\hat{\Sigma}_k^y \triangleq \eta_k^2 \Lambda_{\text{pos}}^{\beta_k} \hat{\Sigma}_{k-1} \Lambda_{\text{pos}}^{\beta_k} + \left( \mathbf{I} - \frac{\eta_k^2}{2} \Lambda_{\text{pos}}^{\beta_k} \right)^2$ . Here, we used  $\tilde{\Sigma}_k^y$ ,  $\hat{\Sigma}_k^y$  and  $\hat{\Sigma}_k$  to avoid confusion with  $\Sigma_k^y$  and  $\Sigma_k$  in the full-batch setting. In this case, if we follow Stephan et al. [2017] and Chen et al. [2014] in assuming  $\varepsilon$  is Gaussian,<sup>4</sup> we have

$$\mathbb{E}_q \left[ \sum_{k=1}^K \log \frac{\pi(\hat{\mathbf{v}}_k)}{\pi(\mathbf{v}_{k-1})} \right] = \sum_{k=1}^K \left[ -\frac{1}{2} \|\boldsymbol{\mu}_k^y\|_2^2 - \frac{1}{2} \text{Tr}(\hat{\Sigma}_k^y) + \frac{d}{2} \right] - \sum_{k=1}^K \left[ \frac{1}{2} \eta_k^2 \text{Tr}(\Sigma_\varepsilon) \right]. \quad (21)$$

The second term of (21) goes to infinity as  $\lim_{K \rightarrow \infty} \sum_{k=1}^K \eta_k^2 = \infty$ . Intuitively, the gradient noise adds to the kinetic energy, and the size of this contribution is proportional to  $\eta_k^2$ . Since this effect is cumulative over all  $K$  steps,  $\eta_k$  has to be reduced at least as  $1/\sqrt{K}$  for the kinetic energy term to go down. However, this contradicts the requirement of last-iterate convergence.

One may wonder why gradient noise does not hurt the convergence of SGLD [Welling and Teh, 2011] or SGMCMC [Ma et al., 2015]. Generally speaking, these algorithms are only concerned with the last iteration convergence to the true posterior, hence one can eliminate stochastic error by taking more steps of a smaller size. In contrast, our bound (and potentially other AIS-style algorithms) relies on all intermediate distributions, and so the error induced by stochastic gradient noise accumulates over the whole trajectory.

## 5 Related Works

For ML estimation (or partition function estimation), Sequential Monte Carlo (SMC) [Doucet et al., 2001, Del Moral et al., 2006] is another popular method which is derived from partial filtering method. While SMC is based on a different intuition from AIS, the underlying mathematics is equivalent. In SMC, the intermediate distributions are defined by conditioning on a sequence of increasing subsets of data. Therefore, we expect our analysis in Section 4 would also apply to SMC.

Besides, both AIS and SMC are closely related to a broader family of techniques for partition function estimation, all based on the following identity from statistical physics:  $\log \mathcal{Z}_K - \log \mathcal{Z}_0 = \int_0^1 \mathbb{E}_{\boldsymbol{\theta} \sim p_\beta} \left[ \frac{d}{d\beta} \log f_\beta(\boldsymbol{\theta}) \right] d\beta$ . In particular, the weight update in AIS can be seen as a finite difference approximation. In comparison, thermodynamic integration (TI) [Frenkel and Smit, 2001] estimates this integration using numerical quadrature, and path sampling [Gelman and Meng, 1998] does so with Monte Carlo integration. Recently, Masrani et al. [2019] connected TI and variational inference for a tighter bound on the log ML. Concurrently, Geffner and Domke [2021] proposed the same algorithm as our DAVI with a focus on the empirical side.

In the context of variational inference, many papers have also investigated tighter lower bounds for the log ML. Burda et al. [2016] proposed a strictly tighter log-likelihood lower bound derived from importance weighting. Salimans et al. [2015] proposed to incorporate MCMC iterations into the variational approximation. However, the proposed methods require learning reverse kernels which have a large impact on performance. The same authors also briefly discussed annealed variational

<sup>4</sup>This assumption is non-essential, though Gaussian noise is reasonable by the central limit theorem.

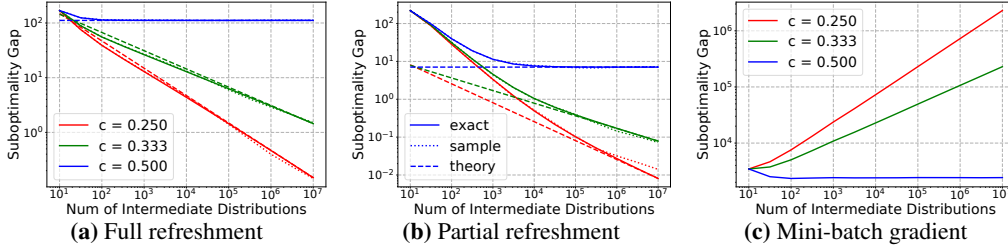


**Figure 1:** Gap between true log ML and our DAIS bound as a function of number of intermediate distributions. Solid lines are exact computation of our DAIS bound; dotted lines are sample-based simulation (Monte Carlo method with 100 samples); dashed lines are theoretical predictions based on Theorem 1 with slope  $2c - 1$ . For the rightmost figure, we use a batch size of 100.

inference, which combines variational inference and AIS. However, their derivation relies on the detailed balance assumption and is therefore not amenable to gradient-based optimization. Later, [Caterini et al. \[2019\]](#) proposed the Hamiltonian VAE, which improves Hamiltonian variational inference [[Salimans et al., 2015](#)] with an optimally chosen reverse MCMC kernel. In particular, they removed the momentum sampling step and used deterministic forward transitions. The resulting algorithm can be thought of as a normalizing flow scheme in which the flow depends explicitly on the target distribution. Along this line, [Le et al. \[2018\]](#), [Naesseth et al. \[2018\]](#), [Maddison et al. \[2017\]](#) proposed to meld variational inference and SMC for time-series models.

Finally, stochastic gradient variants of several MCMC algorithms [[Welling and Teh, 2011](#), [Chen et al., 2014](#), [Ma et al., 2015](#)] have been proposed over the last decade. In particular, they showed that adding the “right amount” of noise to the parameter updates leads to samples from the target posterior as long as the step size is annealed. Importantly, the convergence rates of these algorithms are established in both the full-batch setting [[Dalalyan, 2017](#), [Cheng et al., 2018](#)] and the stochastic setting [[Chen et al., 2015](#), [Teh et al., 2016](#), [Raginsky et al., 2017](#), [Zou et al., 2020](#)]. By contrast, the convergence properties for AIS and related algorithms were largely unknown even for the deterministic case, and it remains largely unexplored whether AIS can be made compatible with stochastic gradients.

## 6 Simulations

In this section, we discuss the experiments used to validate our algorithm and theory. Importantly, we do *not* aim to achieve state-of-the-art on these tasks.

### 6.1 Bayesian Linear Regression

In Section 4, we proved for the Bayesian linear regression setting that while DAIS is asymptotically consistent with full-batch gradient, the noise injected into the system via stochastic gradients precludes convergence. Here, we verify our theory with numerical simulations. The  $n$  input vectors  $\mathbf{X} \in \mathbb{R}^{n \times d}$  and targets  $\mathbf{y} \in \mathbb{R}^n$  respectively consist of entries sampled from  $\mathcal{N}(0, 0.01)$  and  $\mathcal{N}(0, 1)$ . In particular, we choose  $n = 10,000$  and  $d = 10$  for our simulations (the results are qualitatively same with different  $n$  and  $d$ ). In addition, we set the observation variance  $\sigma^2 = 1$ . For convenience, we set the linear annealing scheme  $\beta_k = \frac{k}{K}$ .

In Figure 1, we report the gap between exact log ML and our bound as a function of number of intermediate distributions. With full-batch gradients, the simulations (solid and dotted lines) align well with our theoretical predictions (dashed lines) for different step-size scaling schemes, suggesting our bound in Theorem 1 is tight. In addition, we observe in Figure 1c that the gap fails to vanish with mini-batch gradients for all step-size scaling schemes. Interestingly, with  $c = 1/2$ , the gap stays constant. This matches our predictions that the deterministic error decays as  $\mathcal{O}(K^{2c-1}) = \mathcal{O}(1)$  while the stochastic error is proportional to  $\sum_{k=1}^K \eta_k^2 = \mathcal{O}(K^{2c-1}) = \mathcal{O}(1)$ .

### 6.2 Variational Autoencoder

We compare the performance of DAVI to vanilla VAE [[Kingma and Welling, 2013](#)] and IWAE [[Burda et al., 2016](#)] on density modeling tasks. We use the dynamically binarized MNIST [[LeCun et al., 1998](#)] dataset. We use the same architecture as in IWAE paper. The prior  $p(\mathbf{z})$  is a 50-dimensional



**Table 2:** Test negative log-likelihood of the trained model, estimated using AIS with 10,000 intermediate distribution and 10 particles. For VAE/IWAE, we used  $S \times K$  samples. The numbers reported are averaged over three runs. The standard deviations are fairly small over three runs ( $< 0.06$ ).

Objective	$S \times K = 1$	$S \times K = 5$	$S \times K = 50$			$S \times K = 500$	
	$K = 1$	$K = 5$	$K = 5$	$K = 10$	$K = 50$	$K = 10$	$K = 50$
VAE	86.93	86.95	86.94			86.89	
IWAE	86.93	<b>85.43</b>	84.46			83.87	
DAVI	-	86.51	84.49	84.45	85.23	83.62	83.65
DAVI (adapt)	-	86.49	84.42	<b>84.39</b>	85.00	<b>83.56</b>	83.69

standard Gaussian distribution. The conditional distributions  $p(\mathbf{x}_i|\mathbf{z})$  are independent Bernoulli, with the decoder parameterized by two hidden layers, each with 200 tanh units. The variational posterior  $q(\mathbf{z}|\mathbf{x})$  is also a 50-dimensional Gaussian with diagonal covariance, whose mean and variance are both parameterized by two hidden layers with 200 tanh units (see other details in Appendix C.1).

In the first set of experiments, we investigate the effect of number of intermediate distributions  $K$  and combine it with importance sampling (as done in IWAE) with  $S$  samples in DAVI. To be specific, we define the bound as follows:

$$\log \frac{1}{S} \sum_{i=1}^S \left( \frac{p_{\theta}(\mathbf{x}, \mathbf{z}_K^i)}{q_{\phi}(\mathbf{z}_0^i|\mathbf{x})} \prod_{k=1}^K \frac{\pi(\hat{\mathbf{v}}_k^i)}{\pi(\mathbf{v}_{k-1}^i)} \right), \quad (22)$$

where we sample  $(\mathbf{z}_0^i, \mathbf{v}_0^i, \hat{\mathbf{v}}_1^i, \dots)$  independently from  $q_{\text{fwd}}$ . By default, we use partial momentum refreshment with  $\gamma = 0.9$  and equally spaced annealing parameters  $\beta_k = k/K$ . We compare it to vanilla VAE and IWAE bounds with  $S \times K$  samples. As shown in Table 2, increasing  $K$  gives strictly better models with lower test negative log-likelihood. However, IWAE achieves slightly better performance with roughly the same computation if  $S \times K$  is small. On the other hand, DAVI is more effective with more compute budget (i.e.,  $S \times K$  is large) and eventually outperforms IWAE.

In the second set of experiments, we learn the annealing scheme of DAVI together with the parameters of encoder and decoder. Comparing the third and fourth rows of Table 2, one can see that learning the annealing scheme improves the performance slightly.

Lastly, we also compare our algorithm with IWAE, AIS, and Hamiltonian AIS (HAIS) [Sohl-Dickstein and Culpeper, 2012] in evaluating the log-likelihood of trained models. To be noted, IWAE and AIS have been widely used in evaluating VAE, see e.g. Wu et al. [2016], Huang et al. [2020]. For HAIS and DAIS, we employ the optimal step-size scaling scheme derived in Theorem 1 with  $c = 1/4$  and only tune the step size for the case of  $K = 10$ . For all implementation details, please see Appendix C.2. In particular, we choose the vanilla VAE model to compare all different algorithms (see results of other models in Appendix C.3). In Figure 2, we report the estimated negative log-likelihood as a function of the number of particles (for IWAE) or gradient updates (for AIS, HAIS and DAIS). Interestingly, we observe that IWAE performs better when we have limited computation and AIS/HAIS/DAIS win out if we increase  $K$ . Moreover, DAIS performs on par with AIS/HAIS but without requiring the MH correction steps.

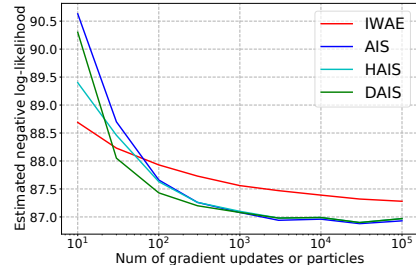


**Figure 2:** Results of different algorithms in evaluating a trained VAE model.

## 7 Conclusion

In this paper, we proposed a differentiable AIS (DAIS) algorithm for marginal likelihood estimation. We provided a detailed convergence analysis for Bayesian linear regression which goes beyond existing analyses. Using this analysis, we proved a sublinear convergence rate of DAIS in the full-batch setting. However, we showed that DAIS is inconsistent when mini-batch gradients are used due to a fundamental incompatibility between the goals of last-iterate convergence to the posterior and elimination of the pathwise stochastic error. This comprises an interesting counterexample to the general trend of algorithms consistent in the deterministic setting remaining consistent in the stochastic setting. Our negative result helps explain the difficulty of developing practically effective AIS-like algorithms that exploit mini-batch gradients. Our numerical experiments validate our claims.

## References

- Charles Blundell, Julien Cornebise, Koray Kavukcuoglu, and Daan Wierstra. Weight uncertainty in neural network. In *International Conference on Machine Learning*, pages 1613–1622. PMLR, 2015.
- Yuri Burda, Roger B Grosse, and Ruslan Salakhutdinov. Importance weighted autoencoders. In *ICLR (Poster)*, 2016.
- AL Caterini, A Doucet, and D Sejdinovic. Hamiltonian variational auto-encoder. *Advances in Neural Information Processing Systems*, 31, 2019.
- Changyou Chen, Nan Ding, and Lawrence Carin. On the convergence of stochastic gradient mcmc algorithms with high-order integrators. In *Proceedings of the 28th International Conference on Neural Information Processing Systems-Volume 2*, pages 2278–2286, 2015.
- Tianqi Chen, Emily Fox, and Carlos Guestrin. Stochastic gradient hamiltonian monte carlo. In *International conference on machine learning*, pages 1683–1691. PMLR, 2014.
- Xiang Cheng, Niladri S Chatterji, Peter L Bartlett, and Michael I Jordan. Underdamped langevin mcmc: A non-asymptotic analysis. In *Conference on Learning Theory*, pages 300–323. PMLR, 2018.
- Arnak S Dalalyan. Theoretical guarantees for approximate sampling from smooth and log-concave densities. *Journal of the Royal Statistical Society: Series B (Statistical Methodology)*, 79(3): 651–676, 2017.
- Pierre Del Moral, Arnaud Doucet, and Ajay Jasra. Sequential monte carlo samplers. *Journal of the Royal Statistical Society: Series B (Statistical Methodology)*, 68(3):411–436, 2006.
- Arnaud Doucet, Nando De Freitas, and Neil Gordon. An introduction to sequential monte carlo methods. In *Sequential Monte Carlo methods in practice*, pages 3–14. Springer, 2001.
- Daan Frenkel and Berend Smit. *Understanding molecular simulation: from algorithms to applications*, volume 1. Elsevier, 2001.
- Tomas Geffner and Justin Domke. Mcmc variational inference via uncorrected hamiltonian annealing. *arXiv preprint arXiv:2107.04150*, 2021.
- Andrew Gelman and Xiao-Li Meng. Simulating normalizing constants: From importance sampling to bridge sampling to path sampling. *Statistical science*, pages 163–185, 1998.
- Roger B Grosse, Chris J Maddison, and Ruslan Salakhutdinov. Annealing between distributions by averaging moments. In *NIPS*, pages 2769–2777. Citeseer, 2013.
- Roger B Grosse, Zoubin Ghahramani, and Ryan P Adams. Sandwiching the marginal likelihood using bidirectional monte carlo. *arXiv preprint arXiv:1511.02543*, 2015.
- Alan M Horowitz. A generalized guided monte carlo algorithm. *Physics Letters B*, 268(2):247–252, 1991.
- Sicong Huang, Alireza Makhzani, Yanshuai Cao, and Roger Grosse. Evaluating lossy compression rates of deep generative models. In *International Conference on Machine Learning*, pages 4444–4454. PMLR, 2020.
- Diederik P Kingma and Jimmy Ba. Adam: A method for stochastic optimization. In *ICLR (Poster)*, 2015.
- Diederik P Kingma and Max Welling. Auto-encoding variational bayes. *arXiv preprint arXiv:1312.6114*, 2013.
- Tuan Anh Le, Maximilian Igl, Tom Rainforth, Tom Jin, and Frank Wood. Auto-encoding sequential monte carlo. In *International Conference on Learning Representations*, 2018.
- Yann LeCun, Léon Bottou, Yoshua Bengio, and Patrick Haffner. Gradient-based learning applied to document recognition. *Proceedings of the IEEE*, 86(11):2278–2324, 1998.

- Xuechen Li, Ting-Kam Leonard Wong, Ricky TQ Chen, and David Duvenaud. Scalable gradients for stochastic differential equations. In *International Conference on Artificial Intelligence and Statistics*, pages 3870–3882. PMLR, 2020.
- Yi-An Ma, Tianqi Chen, and Emily Fox. A complete recipe for stochastic gradient mcmc. *Advances in Neural Information Processing Systems*, 28:2917–2925, 2015.
- Dougal Maclaurin, David Duvenaud, and Ryan Adams. Gradient-based hyperparameter optimization through reversible learning. In *International conference on machine learning*, pages 2113–2122. PMLR, 2015.
- Chris J Maddison, Dieterich Lawson, George Tucker, Nicolas Heess, Mohammad Norouzi, Andriy Mnih, Arnaud Doucet, and Yee Whye Teh. Filtering variational objectives. In *Proceedings of the 31st International Conference on Neural Information Processing Systems*, pages 6576–6586, 2017.
- Vaden Masrani, Tuan Anh Le, and Frank Wood. The thermodynamic variational objective. *arXiv preprint arXiv:1907.00031*, 2019.
- Christian Naesseth, Francisco Ruiz, Scott Linderman, and David Blei. Reparameterization gradients through acceptance-rejection sampling algorithms. In *Artificial Intelligence and Statistics*, pages 489–498. PMLR, 2017.
- Christian Naesseth, Scott Linderman, Rajesh Ranganath, and David Blei. Variational sequential monte carlo. In *International Conference on Artificial Intelligence and Statistics*, pages 968–977. PMLR, 2018.
- Radford M Neal. Annealed importance sampling. *Statistics and computing*, 11(2):125–139, 2001.
- Radford M Neal et al. Mcmc using hamiltonian dynamics. *Handbook of markov chain monte carlo*, 2(11):2, 2011.
- Maxim Raginsky, Alexander Rakhlin, and Matus Telgarsky. Non-convex learning via stochastic gradient langevin dynamics: a nonasymptotic analysis. In *Conference on Learning Theory*, pages 1674–1703. PMLR, 2017.
- Carl Edward Rasmussen. Gaussian processes in machine learning. In *Summer school on machine learning*, pages 63–71. Springer, 2003.
- Danilo Jimenez Rezende, Shakir Mohamed, and Daan Wierstra. Stochastic backpropagation and approximate inference in deep generative models. In *International conference on machine learning*, pages 1278–1286. PMLR, 2014.
- Herbert Robbins and Sutton Monro. A stochastic approximation method. *The annals of mathematical statistics*, pages 400–407, 1951.
- Gareth O Roberts, Richard L Tweedie, et al. Exponential convergence of langevin distributions and their discrete approximations. *Bernoulli*, 2(4):341–363, 1996.
- Yangjun Ruan, Karen Ullrich, Daniel Severo, James Townsend, Ashish Khisti, Arnaud Doucet, Alireza Makhzani, and Chris J Maddison. Improving lossless compression rates via monte carlo bits-back coding. *arXiv preprint arXiv:2102.11086*, 2021.
- Tim Salimans, Diederik Kingma, and Max Welling. Markov chain monte carlo and variational inference: Bridging the gap. In *International Conference on Machine Learning*, pages 1218–1226, 2015.
- John Skilling et al. Nested sampling for general bayesian computation. *Bayesian analysis*, 1(4): 833–859, 2006.
- Jascha Sohl-Dickstein and Benjamin J Culpepper. Hamiltonian annealed importance sampling for partition function estimation. *arXiv preprint arXiv:1205.1925*, 2012.
- M Stephan, Matthew D Hoffman, David M Blei, et al. Stochastic gradient descent as approximate bayesian inference. *Journal of Machine Learning Research*, 18(134):1–35, 2017.

- Yee Whye Teh, Alexandre H Thiery, and Sebastian J Vollmer. Consistency and fluctuations for stochastic gradient langevin dynamics. *Journal of Machine Learning Research*, 17, 2016.
- Max Welling and Yee W Teh. Bayesian learning via stochastic gradient langevin dynamics. In *Proceedings of the 28th international conference on machine learning (ICML-11)*, pages 681–688. Citeseer, 2011.
- Yuhuai Wu, Yuri Burda, Ruslan Salakhutdinov, and Roger Grosse. On the quantitative analysis of decoder-based generative models. *arXiv preprint arXiv:1611.04273*, 2016.
- Guodong Zhang, Shengyang Sun, David Duvenaud, and Roger Grosse. Noisy natural gradient as variational inference. In *International Conference on Machine Learning*, pages 5852–5861. PMLR, 2018.
- Guodong Zhang, Lala Li, Zachary Nado, James Martens, Sushant Sachdeva, George E Dahl, Christopher J Shallue, and Roger Grosse. Which algorithmic choices matter at which batch sizes? insights from a noisy quadratic model. *arXiv preprint arXiv:1907.04164*, 2019.
- Difan Zou, Pan Xu, and Quanquan Gu. Faster convergence of stochastic gradient langevin dynamics for non-log-concave sampling. *arXiv preprint arXiv:2010.09597*, 2020.

## A Proofs

**Lemma 1.** *Given equally spaced  $\beta_k$ , running DAIS with  $\gamma = 0$  and  $\eta \sim \frac{1}{K^c}$  where  $c \geq \frac{1}{4}$  yields*

$$\|\boldsymbol{\mu}_{k-1} - \boldsymbol{\mu}_{\text{pos}}^{\beta_k}\|_2 = \mathcal{O}(K^{2c-1}), \quad \|\boldsymbol{\Lambda}_{k-1} - \boldsymbol{\Lambda}_{\text{pos}}^{\beta_k}\|_2 = \mathcal{O}(K^{2c-1}). \quad (17)$$

*Proof.* We will prove the result for both quantities by induction. We assume  $\boldsymbol{\mu}_p = \mathbf{0}$  and  $\boldsymbol{\Lambda}_p \succeq \mathbf{I}$  without loss of generality and choose  $\eta = \frac{a}{K^c}$ . Recall definitions

$$\boldsymbol{\Lambda}_{\text{lld}} = \frac{1}{\sigma^2} \mathbf{X}^\top \mathbf{X} \quad (23)$$

$$\boldsymbol{\Lambda}_{\text{pos}}^{\beta_k} = \boldsymbol{\Lambda}_p + \beta_k \boldsymbol{\Lambda}_{\text{lld}} \quad (24)$$

$$\boldsymbol{\mu}_* = (\mathbf{X}^\top \mathbf{X})^{-1} \mathbf{X}^\top \mathbf{y} \quad (25)$$

$$\boldsymbol{\mu}_{\text{pos}}^{\beta_k} = (\boldsymbol{\Lambda}_{\text{pos}}^{\beta_k})^{-1} (\boldsymbol{\Lambda}_p \boldsymbol{\mu}_p + \beta_k \boldsymbol{\Lambda}_{\text{lld}} \boldsymbol{\mu}_*). \quad (26)$$

We first bound intermediate quantities of interest. In particular, we have

$$\begin{aligned} \|\boldsymbol{\Sigma}_{\text{pos}}^{\beta_{k-1}} - \boldsymbol{\Sigma}_{\text{pos}}^{\beta_k}\|_2 &\leq \|\boldsymbol{\Sigma}_{\text{pos}}^{\beta_{k-1}}\|_2 \|\boldsymbol{\Lambda}_{\text{pos}}^{\beta_{k-1}} - \boldsymbol{\Lambda}_{\text{pos}}^{\beta_k}\|_2 \|\boldsymbol{\Sigma}_{\text{pos}}^{\beta_k}\|_2 \\ &= (\beta_k - \beta_{k-1}) \|\boldsymbol{\Sigma}_{\text{pos}}^{\beta_{k-1}}\|_2 \|\boldsymbol{\Lambda}_{\text{lld}}\|_2 \|\boldsymbol{\Sigma}_{\text{pos}}^{\beta_k}\|_2 \\ &= \frac{C_3}{K} \end{aligned} \quad (27)$$

and

$$\begin{aligned} \|\boldsymbol{\mu}_{\text{pos}}^{\beta_{k-1}} - \boldsymbol{\mu}_{\text{pos}}^{\beta_k}\|_2 &= \|\boldsymbol{\Sigma}_{\text{pos}}^{\beta_{k-1}} \beta_{k-1} \boldsymbol{\Lambda}_{\text{lld}} \boldsymbol{\mu}_* - \boldsymbol{\Sigma}_{\text{pos}}^{\beta_k} \beta_k \boldsymbol{\Lambda}_{\text{lld}} \boldsymbol{\mu}_*\|_2 \\ &\leq \|(\beta_k \boldsymbol{\Sigma}_{\text{pos}}^{\beta_k} - \beta_{k-1} \boldsymbol{\Sigma}_{\text{pos}}^{\beta_{k-1}})\|_2 \|\boldsymbol{\Lambda}_{\text{lld}} \boldsymbol{\mu}_*\|_2 \\ &= \|\beta_k (\boldsymbol{\Sigma}_{\text{pos}}^{\beta_k} - \boldsymbol{\Sigma}_{\text{pos}}^{\beta_{k-1}}) + (\beta_k - \beta_{k-1}) \boldsymbol{\Sigma}_{\text{pos}}^{\beta_{k-1}}\|_2 \|\boldsymbol{\Lambda}_{\text{lld}} \boldsymbol{\mu}_*\|_2 \\ &\leq \left( \beta_k \|\boldsymbol{\Sigma}_{\text{pos}}^{\beta_k} - \boldsymbol{\Sigma}_{\text{pos}}^{\beta_{k-1}}\|_2 + (\beta_k - \beta_{k-1}) \|\boldsymbol{\Sigma}_{\text{pos}}^{\beta_{k-1}}\|_2 \right) \|\boldsymbol{\Lambda}_{\text{lld}} \boldsymbol{\mu}_*\|_2 \\ &= \left( \beta_k \frac{C_3}{K} + (\beta_k - \beta_{k-1}) \|\boldsymbol{\Sigma}_{\text{pos}}^{\beta_{k-1}}\|_2 \right) \|\boldsymbol{\Lambda}_{\text{lld}} \boldsymbol{\mu}_*\|_2 \\ &= \frac{C_1}{K} \end{aligned} \quad (28)$$

We now begin the induction for  $\|\boldsymbol{\mu}_{k-1} - \boldsymbol{\mu}_{\text{pos}}^{\beta_k}\|_2$ . For  $k = 1$ , we have  $\boldsymbol{\mu}_0 = \boldsymbol{\mu}_p$  and obtain

$$\|\boldsymbol{\mu}_0 - \boldsymbol{\mu}_{\text{pos}}^{\beta_1}\|_2 = \|\boldsymbol{\mu}_{\text{pos}}^{\beta_0} - \boldsymbol{\mu}_{\text{pos}}^{\beta_1}\|_2 = \mathcal{O}(K^{-1}). \quad (29)$$

Next, we assume  $\|\boldsymbol{\mu}_{k-1} - \boldsymbol{\mu}_{\text{pos}}^{\beta_k}\|_2 = C_2 K^{2c-1} = \mathcal{O}(K^{2c-1})$  holds for  $k \geq 1$ . Subtracting  $\boldsymbol{\mu}_{\text{pos}}^{\beta_k}$  from both sides of (72) yields

$$\boldsymbol{\mu}_k - \boldsymbol{\mu}_{\text{pos}}^{\beta_k} = \left( \mathbf{I} - \frac{\eta_k^2}{2} \boldsymbol{\Lambda}_{\text{pos}}^{\beta_k} \right) (\boldsymbol{\mu}_{k-1} - \boldsymbol{\mu}_{\text{pos}}^{\beta_k}). \quad (30)$$

As  $\boldsymbol{\Lambda}_{\text{pos}}^{\beta_k} \succeq \boldsymbol{\Lambda}_p \succeq \mathbf{I}$  by construction, we have

$$\begin{aligned} \|\boldsymbol{\mu}_k - \boldsymbol{\mu}_{\text{pos}}^{\beta_{k+1}}\|_2 &\leq \|\boldsymbol{\mu}_k - \boldsymbol{\mu}_{\text{pos}}^{\beta_k}\|_2 + \|\boldsymbol{\mu}_{\text{pos}}^{\beta_k} - \boldsymbol{\mu}_{\text{pos}}^{\beta_{k+1}}\|_2 \\ &\leq \left(1 - \frac{\eta^2}{2}\right) \|\boldsymbol{\mu}_{k-1} - \boldsymbol{\mu}_{\text{pos}}^{\beta_k}\|_2 + \frac{C_1}{K} \\ &= C_2 K^{2c-1} - \frac{a^2 C_2}{2} K^{-1} + C_1 K^{-1} \end{aligned} \quad (31)$$

We have the flexibility to choose  $a$  such that  $a^2 C_2 \geq 2C_1$ , hence we have  $\|\boldsymbol{\mu}_k - \boldsymbol{\mu}_{\text{pos}}^{\beta_{k+1}}\|_2 \leq C_2 K^{2c-1}$ . This completes the proof for  $\|\boldsymbol{\mu}_{k-1} - \boldsymbol{\mu}_{\text{pos}}^{\beta_k}\|_2$ .

Now, we bound  $\|\mathbf{\Lambda}_{k-1} - \mathbf{\Lambda}_{\text{pos}}^{\beta_k}\|_2$ . It suffices to prove that  $\|\mathbf{\Sigma}_{k-1} - \mathbf{\Sigma}_{\text{pos}}^{\beta_k}\|_2 = \mathcal{O}(K^{2c-1})$  because  $\|\mathbf{\Lambda}_{k-1} - \mathbf{\Lambda}_{\text{pos}}^{\beta_k}\|_2 \leq \|\mathbf{\Lambda}_{k-1}\|_2 \|\mathbf{\Sigma}_{k-1} - \mathbf{\Sigma}_{\text{pos}}^{\beta_k}\|_2 \|\mathbf{\Lambda}_{\text{pos}}^{\beta_k}\|_2$ . For  $k = 1$ , we have  $\mathbf{\Sigma}_0 = \mathbf{\Sigma}_p$  and obtain

$$\|\mathbf{\Sigma}_0 - \mathbf{\Sigma}_{\text{pos}}^{\beta_1}\|_2 = \|\mathbf{\Sigma}_{\text{pos}}^{\beta_0} - \mathbf{\Sigma}_{\text{pos}}^{\beta_1}\|_2 = \mathcal{O}(K^{-1}) \quad (32)$$

by (27). Next, we assume  $\|\mathbf{\Sigma}_{k-1} - \mathbf{\Sigma}_{\text{pos}}^{\beta_k}\|_2 \leq C_4 K^{2c-1}$  for  $k \geq 1$ . Subtracting  $\mathbf{\Sigma}_{\text{pos}}^{\beta_{k+1}}$  from both sides of (74) yields

$$\begin{aligned} \mathbf{\Sigma}_k - \mathbf{\Sigma}_{\text{pos}}^{\beta_{k+1}} &= \left( \mathbf{I} - \frac{\eta^2}{2} \mathbf{\Lambda}_{\text{pos}}^{\beta_k} \right) (\mathbf{\Sigma}_{k-1} - \mathbf{\Sigma}_{\text{pos}}^{\beta_k}) \left( \mathbf{I} - \frac{\eta^2}{2} \mathbf{\Lambda}_{\text{pos}}^{\beta_k} \right) \\ &\quad + \mathbf{\Sigma}_{\text{pos}}^{\beta_k} - \mathbf{\Sigma}_{\text{pos}}^{\beta_{k+1}} - \frac{\eta^4}{4} \mathbf{\Lambda}_{\text{pos}}^{\beta_k} + \frac{\eta^6}{16} (\mathbf{\Lambda}_{\text{pos}}^{\beta_k})^2. \end{aligned} \quad (33)$$

By invoking  $\mathbf{\Lambda}_{\text{pos}}^{\beta_k} \succeq \mathbf{I}$ , we have

$$\begin{aligned} \|\mathbf{\Sigma}_k - \mathbf{\Sigma}_{\text{pos}}^{\beta_{k+1}}\|_2 &\leq \left( 1 - \frac{\eta^2}{2} \right)^2 \|\mathbf{\Sigma}_{k-1} - \mathbf{\Sigma}_{\text{pos}}^{\beta_k}\|_2 + \|\mathbf{\Sigma}_{\text{pos}}^{\beta_k} - \mathbf{\Sigma}_{\text{pos}}^{\beta_{k+1}}\|_2 + \frac{\eta^4}{4} \left\| \mathbf{\Lambda}_{\text{pos}}^{\beta_k} - \frac{\eta^2}{4} (\mathbf{\Lambda}_{\text{pos}}^{\beta_k})^2 \right\|_2 \\ &\leq C_4 K^{2c-1} - a^2 C_4 K^{-1} + \frac{a^4 C_4}{4} K^{-2c-1} + C_3 K^{-1} + a^4 C_5 K^{-4c}. \end{aligned} \quad (34)$$

To finish the proof, we can choose  $a$  and  $C_4$  to ensure  $a^2 C_4 - C_3 - a^4 C_5 - \frac{a^4 C_4}{4} > 0$ .  $\square$

**Theorem 1.** *Given equally spaced  $\beta_k$ , running DAIS with  $\gamma = 0$  and  $\eta \sim \frac{1}{K^c}$  where  $c \geq \frac{1}{4}$  yields*

$$\log p(\mathcal{D}) - \mathcal{L}_{\text{DAIS}} = \mathcal{O}(K^{2c-1}).$$

With  $c = \frac{1}{4}$ , we have the optimal convergence rate  $\mathcal{O}(1/\sqrt{K})$ .

*Proof.* By Lemma 1, we have the first two terms in (16) upper bounded as follows,

$$\begin{aligned} \left| \frac{1}{2} \|\boldsymbol{\mu}_K - \boldsymbol{\mu}_{\text{pos}}\|_{\mathbf{\Lambda}_{\text{pos}}}^2 + \frac{1}{2} \text{Tr}(\mathbf{\Lambda}_{\text{pos}} \boldsymbol{\Sigma}_K) - \frac{d}{2} \right| &\leq \frac{1}{2} \|\boldsymbol{\mu}_K - \boldsymbol{\mu}_{\text{pos}}\|_{\mathbf{\Lambda}_{\text{pos}}}^2 + \frac{1}{2} |\text{Tr}(\mathbf{\Lambda}_{\text{pos}} (\boldsymbol{\Sigma}_K - \mathbf{\Sigma}_{\text{pos}}))| \\ &= \mathcal{O}(K^{4c-2}) + \mathcal{O}(K^{2c-1}) = \mathcal{O}(K^{2c-1}) \end{aligned} \quad (35)$$

where we use the identity that  $|\text{Tr}(\mathbf{A}\mathbf{B})| \leq d \|\mathbf{A}\|_2 \|\mathbf{B}\|_2$ .

Now, it suffices to show the term ③ vanishes as  $K \rightarrow \infty$ . To put it differently, we only need to show that  $\lim_{K \rightarrow \infty} \mathbb{E}_q \left[ \sum_{k=1}^K \log \frac{\pi(\hat{\mathbf{v}}_k)}{\pi(\mathbf{v}_{k-1})} \right] = \frac{1}{2} \log \frac{|\mathbf{\Sigma}_{\text{pos}}|}{|\mathbf{\Sigma}_p|}$ . To this end, we could first simplify  $\mathbb{E}_q \left[ \sum_{k=1}^K \log \frac{\pi(\hat{\mathbf{v}}_k)}{\pi(\mathbf{v}_{k-1})} \right]$  as we know  $\hat{\mathbf{v}}_k$  follows a Gaussian distribution  $\mathcal{N}(\boldsymbol{\mu}_k^{\mathbf{v}}, \boldsymbol{\Sigma}_k^{\mathbf{v}})$ .

$$\mathbb{E}_q \left[ \sum_{k=1}^K \log \frac{\pi(\hat{\mathbf{v}}_k)}{\pi(\mathbf{v}_{k-1})} \right] = \sum_{k=1}^K \left[ -\frac{1}{2} \|\boldsymbol{\mu}_k^{\mathbf{v}}\|_2^2 - \frac{1}{2} \text{Tr}(\boldsymbol{\Sigma}_k^{\mathbf{v}}) + \frac{d}{2} \right] \quad (36)$$

According to (15), we have  $\boldsymbol{\mu}_k^{\mathbf{v}} = -\eta \mathbf{\Lambda}_{\text{pos}}^{\beta_k} (\boldsymbol{\mu}_k - \boldsymbol{\mu}_{\text{pos}}^{\beta_k})$ . Then by Lemma 1, we obtain  $\|\boldsymbol{\mu}_k^{\mathbf{v}}\|_2^2 = \mathcal{O}(K^{2c-2})$  and  $\sum_{k=1}^K \left[ \frac{1}{2} \|\boldsymbol{\mu}_k^{\mathbf{v}}\|_2^2 \right] = \mathcal{O}(K^{2c-1})$ . Again, this term would vanish if we choose  $c < \frac{1}{2}$ . From (76), we can write  $\text{Tr}(\boldsymbol{\Sigma}_k^{\mathbf{v}})$  as

$$\begin{aligned} \text{Tr}(\boldsymbol{\Sigma}_k^{\mathbf{v}}) &= \text{Tr} \left( \eta^2 \mathbf{\Lambda}_{\text{pos}}^{\beta_k} \boldsymbol{\Sigma}_{k-1} \mathbf{\Lambda}_{\text{pos}}^{\beta_k} + \left( \mathbf{I} - \frac{\eta^2}{2} \mathbf{\Lambda}_{\text{pos}}^{\beta_k} \right)^2 \right) \\ &= \eta^2 \text{Tr} \left( \mathbf{\Lambda}_{\text{pos}}^{\beta_k} \boldsymbol{\Sigma}_{k-1} (\mathbf{\Lambda}_{\text{pos}}^{\beta_k} - \mathbf{\Lambda}_{k-1}) \right) + d + \frac{\eta^4}{4} \text{Tr} \left( (\mathbf{\Lambda}_{\text{pos}}^{\beta_k})^2 \right) \end{aligned} \quad (37)$$

In addition, we have the recurrence for  $\boldsymbol{\Sigma}_k$ :

$$\boldsymbol{\Sigma}_k = \left( \mathbf{I} - \frac{1}{2} \eta^2 \mathbf{\Lambda}_{\text{pos}}^{\beta_k} \right) \boldsymbol{\Sigma}_{k-1} \left( \mathbf{I} - \frac{1}{2} \eta^2 \mathbf{\Lambda}_{\text{pos}}^{\beta_k} \right) + \eta^2 \left( \mathbf{I} - \frac{1}{2} \eta^2 \mathbf{\Lambda}_{\text{pos}}^{\beta_k} + \frac{\eta^4}{16} (\mathbf{\Lambda}_{\text{pos}}^{\beta_k})^2 \right) \quad (38)$$

This immediately leads to

$$\begin{aligned} \text{Tr}((\Sigma_k - \Sigma_{k-1})\Lambda_{\text{pos}}^{\beta_k}) &= -\eta^2 \text{Tr}(\Lambda_{\text{pos}}^{\beta_k} \Sigma_{k-1} (\Lambda_{\text{pos}}^{\beta_k} - \Lambda_{k-1})) \\ &\quad + \frac{\eta^4}{4} \text{Tr}(\Lambda_{\text{pos}}^{\beta_k} \Sigma_{k-1} (\Lambda_{\text{pos}}^{\beta_k})^2) - \frac{\eta^4}{2} \text{Tr}((\Lambda_{\text{pos}}^{\beta_k})^2) + \frac{\eta^6}{16} \text{Tr}((\Lambda_{\text{pos}}^{\beta_k})^3) \end{aligned} \quad (39)$$

where we used the identity  $\text{Tr}(\mathbf{AB}) = \text{Tr}(\mathbf{BA})$ . Plugging (39) back into (37), we have

$$\text{Tr}(\Sigma_k^{\mathbf{y}}) = d - \text{Tr}((\Sigma_k - \Sigma_{k-1})\Lambda_{\text{pos}}^{\beta_k}) + \frac{\eta^4}{4} \text{Tr}((\Lambda_{\text{pos}}^{\beta_k} - \Lambda_{k-1})\Sigma_{k-1}(\Lambda_{\text{pos}}^{\beta_k})^2) + \frac{\eta^6}{16} \text{Tr}((\Lambda_{\text{pos}}^{\beta_k})^3) \quad (40)$$

Further, if we sum over all timesteps, we get

$$\begin{aligned} \sum_{k=1}^K \left[ -\frac{1}{2} \text{Tr}(\Sigma_k^{\mathbf{y}}) + \frac{d}{2} \right] &= \\ &\quad \underbrace{\frac{1}{2} \sum_{k=1}^K [\text{Tr}((\Sigma_k - \Sigma_{k-1})\Lambda_{k-1})]}_{=\frac{1}{2} \log \frac{|\Sigma_K|}{|\Sigma_p|} + \mathcal{O}(K^{-1})} + \underbrace{\frac{1}{2} \sum_{k=1}^K [\text{Tr}((\Sigma_k - \Sigma_{k-1})(\Lambda_{\text{pos}}^{\beta_k} - \Lambda_{k-1}))]}_{=\mathcal{O}(K^{2c-1})} \\ &\quad - \underbrace{\frac{\eta^4}{8} \sum_{k=1}^K [\text{Tr}((\Lambda_{\text{pos}}^{\beta_k} - \Lambda_{k-1})\Sigma_{k-1}(\Lambda_{\text{pos}}^{\beta_k})^2)]}_{=\mathcal{O}(K^{-2c})} - \underbrace{\frac{\eta^6}{32} \sum_{k=1}^K [\text{Tr}((\Lambda_{\text{pos}}^{\beta_k})^3)]}_{=\mathcal{O}(K^{-6c+1})} \end{aligned} \quad (41)$$

For the first term, we used the Riemann sum approximation for the integral

$$\int_{\Sigma_p}^{\Sigma_K} \text{Tr}(\Sigma^{-1} d\Sigma) = \int_{\Sigma_p}^{\Sigma_K} d \log |\Sigma| = \log |\Sigma_K| - \log |\Sigma_p|. \quad (42)$$

Importantly, the integral is independent of the path  $\Sigma(t)$  and we could choose the path to go through all  $\Sigma_k$ . By the same argument of Riemann sum, the approximation error is bounded by  $\mathcal{O}\left(\sum_{k=1}^K \|\Sigma_k - \Sigma_{k-1}\|_2^2\right)$ . By (74), one can show that  $\|\Sigma_k - \Sigma_{k-1}\|_2 = \mathcal{O}(K^{-1})$ , so we have the approximation error  $\mathcal{O}(K^{-1})$ . For the second term, we used that fact that  $|\text{Tr}(\mathbf{AB})| \leq d\|\mathbf{A}\|_2\|\mathbf{B}\|_2$ . Therefore, the whole term will converge to  $\frac{1}{2} \log \frac{|\Sigma_K|}{|\Sigma_p|}$  if  $\frac{1}{4} \leq c < \frac{1}{2}$ . Finally, by Lemma 1, we have

$$\log \frac{|\Sigma_K|}{|\Sigma_p|} = \log \frac{|\Sigma_{\text{pos}}|}{|\Sigma_p|} + \log \frac{|\Lambda_{\text{pos}}|}{|\Lambda_K|} = \log \frac{|\Sigma_{\text{pos}}|}{|\Sigma_p|} + \mathcal{O}(K^{2c-1}) \quad (43)$$

Hence, we have ③ =  $\mathcal{O}(K^{2c-1})$  if  $c \geq \frac{1}{4}$ . Therefore, we have

$$\log p(\mathcal{D}) - \mathcal{L}_{\text{DAIS}} = \textcircled{1} + \textcircled{2} + \textcircled{3} = \mathcal{O}(K^{2c-1}). \quad (44)$$

This completes the proof.  $\square$

**Theorem 2.** For stochastic DAIS with full momentum refreshment ( $\gamma = 0$  in Algorithm 1) and any stepsize scheme, we have

$$\liminf_{K \rightarrow \infty} |\log p(\mathcal{D}) - \mathcal{L}_{\text{DAIS}}| > 0. \quad (19)$$

*Proof.* Recall the suboptimality gap

$$\begin{aligned} \log p(\mathcal{D}) - \mathcal{L}_{\text{DAIS}} &= \\ &\quad \underbrace{\frac{1}{2} \|\mu_K - \mu_{\text{pos}}\|_{\Lambda_{\text{pos}}}^2}_{\textcircled{1}} + \underbrace{\frac{1}{2} \text{Tr}(\Lambda_{\text{pos}} \Sigma_K) - \frac{d}{2}}_{\textcircled{2}} + \underbrace{\frac{1}{2} \log \frac{|\Sigma_{\text{pos}}|}{|\Sigma_p|} - \mathbb{E}_q \left[ \sum_{k=1}^K \log \frac{\pi(\hat{\mathbf{v}}_k)}{\pi(\mathbf{v}_{k-1})} \right]}_{\textcircled{3}}. \end{aligned} \quad (45)$$

First, we note that ① would stay unchanged for DAIS with stochastic gradient because  $\mu_K$  is independent of gradient noise. Second, the term ② would only become larger if we use stochastic

gradient because more noise is injected into the system. It is easy for one to show that  $\hat{\Sigma}_k \succeq \Sigma_k$  where  $\hat{\Sigma}_k$  is the covariance of  $\theta_k$  when stochastic gradient is used ( $\Sigma_k$  is the covariance of  $\theta_k$  in the full-batch setting). We will prove this by induction. By (18) and (15), we have

$$\hat{\Sigma}_k = \left(\mathbf{I} - \frac{\eta^2}{2} \Lambda_{\text{pos}}^{\beta_k}\right) \hat{\Sigma}_{k-1} \left(\mathbf{I} - \frac{\eta^2}{2} \Lambda_{\text{pos}}^{\beta_k}\right) + \eta^2 \left(\mathbf{I} - \frac{\eta^2}{2} \Lambda_{\text{pos}}^{\beta_k} + \frac{\eta^4}{16} (\Lambda_{\text{pos}}^{\beta_k})^2\right) + \frac{\eta^4}{4} \Sigma_\varepsilon \quad (46)$$

$$\Sigma_k = \left(\mathbf{I} - \frac{\eta^2}{2} \Lambda_{\text{pos}}^{\beta_k}\right) \Sigma_{k-1} \left(\mathbf{I} - \frac{\eta^2}{2} \Lambda_{\text{pos}}^{\beta_k}\right) + \eta^2 \left(\mathbf{I} - \frac{\eta^2}{2} \Lambda_{\text{pos}}^{\beta_k} + \frac{\eta^4}{16} (\Lambda_{\text{pos}}^{\beta_k})^2\right) \quad (47)$$

At  $k = 1$ , we know  $\hat{\Sigma}_0 = \Sigma_0 = \Sigma_p$ , so we retrieve the base case  $\hat{\Sigma}_1 - \Sigma_1 = \frac{\eta^4}{4} \Sigma_\varepsilon \succeq 0$ . Now assume  $\hat{\Sigma}_{k-1} \succeq \Sigma_{k-1}$ , then

$$\hat{\Sigma}_k - \Sigma_k = \underbrace{\left(\mathbf{I} - \frac{\eta^2}{2} \Lambda_{\text{pos}}^{\beta_k}\right) (\hat{\Sigma}_{k-1} - \Sigma_{k-1}) \left(\mathbf{I} - \frac{\eta^2}{2} \Lambda_{\text{pos}}^{\beta_k}\right)}_{\succeq 0} + \frac{\eta^4}{4} \Sigma_\varepsilon \succeq 0 \quad (48)$$

which completes the induction.

Therefore, we only need to compare ③ of the stochastic gradient variant to its deterministic counterpart. It suffices to show that ③ becomes larger once we use stochastic gradient for the updates. To this end, we let  $\tilde{\Sigma}_k^{\mathbf{v}}$  to be the covariance of  $\hat{\mathbf{v}}_k$  and have the following recursion (by (18))

$$\tilde{\Sigma}_k^{\mathbf{v}} = \eta_k^2 \Lambda_{\text{pos}}^{\beta_k} \hat{\Sigma}_{k-1} \Lambda_{\text{pos}}^{\beta_k} + \left(\mathbf{I} - \frac{\eta_k^2}{2} \Lambda_{\text{pos}}^{\beta_k}\right)^2 + \eta_k^2 \Sigma_\varepsilon. \quad (49)$$

For notational convenience, we let  $\hat{\Sigma}_k^{\mathbf{v}} \triangleq \eta_k^2 \Lambda_{\text{pos}}^{\beta_k} \hat{\Sigma}_{k-1} \Lambda_{\text{pos}}^{\beta_k} + \left(\mathbf{I} - \frac{\eta_k^2}{2} \Lambda_{\text{pos}}^{\beta_k}\right)^2$ . Here, we used  $\tilde{\Sigma}_k^{\mathbf{v}}$ ,  $\hat{\Sigma}_k^{\mathbf{v}}$  and  $\hat{\Sigma}_k$  to avoid confusion with  $\Sigma_k^{\mathbf{v}}$  and  $\Sigma_k$  in the full-batch setting. For convenience, we further assume  $\varepsilon$  is Gaussian (appealing to the central limit theorem) and get

$$\mathbb{E}_q \left[ \sum_{k=1}^K \log \frac{\pi(\hat{\mathbf{v}}_k)}{\pi(\mathbf{v}_{k-1})} \right] = \sum_{k=1}^K \left[ -\frac{1}{2} \|\boldsymbol{\mu}_k^{\mathbf{v}}\|_2^2 - \frac{1}{2} \text{Tr}(\hat{\Sigma}_k^{\mathbf{v}}) + \frac{d}{2} \right] - \sum_{k=1}^K \left[ \frac{1}{2} \eta_k^2 \text{Tr}(\Sigma_\varepsilon) \right]. \quad (50)$$

Importantly, we notice that  $\tilde{\Sigma}_k^{\mathbf{v}} \succeq \Sigma_k^{\mathbf{v}}$  because  $\hat{\Sigma}_k \succeq \Sigma_k$ . So the suboptimality gap (45) increases at least by  $\sum_{k=1}^K \left[ \frac{1}{2} \eta_k^2 \text{Tr}(\Sigma_\varepsilon) \right]$  with stochastic gradient update in DAIS. This immediately implies the necessary condition of DAIS being consistent is

$$\lim_{K \rightarrow \infty} \sum_{k=1}^K \eta_k^2 = 0, \quad (51)$$

where we assume  $\text{Tr}(\Sigma_\varepsilon) > 0$ . We now show that for  $\boldsymbol{\mu}_K$  to converge to posterior mean  $\boldsymbol{\mu}_{\text{pos}}$  (so that ① vanishes), a major requirement is  $\lim_{K \rightarrow \infty} \sum_{k=1}^K \eta_k^2 = \infty$ . To prove that, we observe that the mean of  $\theta_k$  evolves as follows:

$$\boldsymbol{\mu}_k - \boldsymbol{\mu}_{\text{pos}}^{\beta_k} \leftarrow \left(\mathbf{I} - \frac{\eta_k^2}{2} \Lambda_{\text{pos}}^{\beta_k}\right) (\boldsymbol{\mu}_{k-1} - \boldsymbol{\mu}_{\text{pos}}^{\beta_k}) \quad (52)$$

Since  $\eta_k$  is  $o(1)$  by (51) and we know  $\Lambda_{\text{pos}}^{\beta_k}$  is upper bounded by  $C\mathbf{I}$  for some constant  $C$ . One can show the following by induction:

$$\|\boldsymbol{\mu}_K - \boldsymbol{\mu}_{\text{pos}}\|_2 \geq \left\| \left( \prod_{k=1}^K \left(1 - \frac{C\eta_k^2}{2}\right) \right) (\boldsymbol{\mu}_0 - \boldsymbol{\mu}_{\text{pos}}) \right\|_2 \quad (53)$$

For  $\|\boldsymbol{\mu}_K - \boldsymbol{\mu}_{\text{pos}}\|_2 \rightarrow 0$  in the worst case, it requires the following to hold:

$$\lim_{K \rightarrow \infty} \prod_{k=1}^K \left(1 - \frac{C\eta_k^2}{2}\right) = 0. \quad (54)$$

This is equivalent to

$$\lim_{K \rightarrow \infty} \sum_{k=1}^K \log \left(1 - \frac{C\eta_k^2}{2}\right) \stackrel{\eta_k = o(1)}{\approx} - \lim_{K \rightarrow \infty} \sum_{k=1}^K \frac{C\eta_k^2}{2} = -\infty \quad (55)$$

This completes the proof.  $\square$



## B Other Derivations

### B.1 DAIS Update

Here, we derive the DAIS updates for the position and (pre-refreshment) momentum of the parameter particles for the Bayesian linear regression setting. Recall that the update from step  $k-1$  to step  $k$  takes the general form

$$\boldsymbol{\theta}_{k-\frac{1}{2}} = \boldsymbol{\theta}_{k-1} + \frac{\eta}{2} \mathbf{M}^{-1} \mathbf{v}_{k-1} \quad (56)$$

$$\hat{\mathbf{v}}_k = \mathbf{v}_{k-1} + \eta \nabla \log f_{\beta_k}(\boldsymbol{\theta}_{k-\frac{1}{2}}) \quad (57)$$

$$\boldsymbol{\theta}_k = \boldsymbol{\theta}_{k-\frac{1}{2}} + \frac{\eta}{2} \mathbf{M}^{-1} \hat{\mathbf{v}}_k \quad (58)$$

Under a geometric annealing scheme, the log annealed unnormalized posterior at step  $k$  has the form

$$\begin{aligned} \log f_{\beta_k}(\boldsymbol{\theta}) &= \log(p(\boldsymbol{\theta}|\mathcal{M})p(\mathcal{D}|\boldsymbol{\theta}, \mathcal{M})^{\beta_k}) \\ &= -\frac{1}{2}(\boldsymbol{\theta} - \boldsymbol{\mu}_p)^\top \boldsymbol{\Lambda}_p (\boldsymbol{\theta} - \boldsymbol{\mu}_p) - \frac{\beta_k}{2\sigma^2} (\mathbf{y} - \mathbf{X}\boldsymbol{\theta})^\top (\mathbf{y} - \mathbf{X}\boldsymbol{\theta}) + C, \end{aligned} \quad (59)$$

where  $C$  comprises terms constant w.r.t.  $\boldsymbol{\theta}$ . The gradient of this is then

$$\nabla_{\boldsymbol{\theta}} \log f_{\beta_k}(\boldsymbol{\theta}) = -\boldsymbol{\Lambda}_p (\boldsymbol{\theta} - \boldsymbol{\mu}_p) + \frac{\beta_k}{\sigma^2} \mathbf{X}^\top (\mathbf{y} - \mathbf{X}\boldsymbol{\theta}). \quad (60)$$

Substituting, we have

$$\begin{aligned} \nabla_{\boldsymbol{\theta}_{k-\frac{1}{2}}} \log f_{\beta_k}(\boldsymbol{\theta}_{k-\frac{1}{2}}) &= -\boldsymbol{\Lambda}_p \left( \boldsymbol{\theta}_{k-1} + \frac{\eta_k}{2} \mathbf{v}_{k-1} - \boldsymbol{\mu}_p \right) \\ &\quad + \frac{\beta_k}{\sigma^2} \mathbf{X}^\top \left( \mathbf{y} - \mathbf{X} \left( \boldsymbol{\theta}_{k-1} + \frac{\eta_k}{2} \mathbf{v}_{k-1} \right) \right) \end{aligned} \quad (61)$$

Define the likelihood precision, annealed posterior precision, and annealed posterior mean as

$$\boldsymbol{\Lambda}_{\text{lld}} = \frac{1}{\sigma^2} \mathbf{X}^\top \mathbf{X} \quad (62)$$

$$\boldsymbol{\Lambda}_{\text{pos}}^{\beta_k} = \boldsymbol{\Lambda}_p + \beta_k \boldsymbol{\Lambda}_{\text{lld}} = \boldsymbol{\Lambda}_p + \frac{\beta_k}{\sigma^2} \mathbf{X}^\top \mathbf{X} \quad (63)$$

$$\boldsymbol{\mu}_{\text{pos}}^{\beta_k} = (\boldsymbol{\Lambda}_{\text{pos}}^{\beta_k})^{-1} \left( \boldsymbol{\Lambda}_p \boldsymbol{\mu}_p + \beta_k \boldsymbol{\Lambda}_{\text{lld}} (\mathbf{X}^\top \mathbf{X})^{-1} \mathbf{X}^\top \mathbf{y} \right). \quad (64)$$

For the updated pre-refreshment momentum, we have

$$\begin{aligned} \hat{\mathbf{v}}_k &= \mathbf{v}_{k-1} + \eta_k \nabla_{\boldsymbol{\theta}_{k-\frac{1}{2}}} \log f_{\beta_k}(\boldsymbol{\theta}_{k-\frac{1}{2}}) \\ &= \mathbf{v}_{k-1} - \eta_k \boldsymbol{\Lambda}_p \boldsymbol{\theta}_{k-1} - \frac{\eta_k^2}{2} \boldsymbol{\Lambda}_p \mathbf{v}_{k-1} + \eta_k \boldsymbol{\Lambda}_p \boldsymbol{\mu}_p \\ &\quad + \frac{\beta_k \eta_k}{\sigma^2} \mathbf{X}^\top \mathbf{y} - \frac{\beta_k \eta_k}{\sigma^2} \mathbf{X}^\top \mathbf{X} \boldsymbol{\theta}_{k-1} + \frac{\beta_k \eta_k^2}{2\sigma^2} \mathbf{X}^\top \mathbf{X} \mathbf{v}_{k-1} \\ &= \left( \mathbf{I} - \frac{\eta_k^2}{2} \left( \boldsymbol{\Lambda}_p + \frac{\beta_k}{\sigma^2} \mathbf{X}^\top \mathbf{X} \right) \right) \mathbf{v}_{k-1} - \eta_k \left( \boldsymbol{\Lambda}_p + \frac{\beta_k}{\sigma^2} \mathbf{X}^\top \mathbf{X} \right) \boldsymbol{\theta}_{k-1} \\ &\quad + \eta_k \left( \boldsymbol{\Lambda}_p \boldsymbol{\mu}_p + \frac{\beta_k}{\sigma^2} \mathbf{X}^\top \mathbf{y} \right) \\ &= \left( \mathbf{I} - \frac{\eta_k^2}{2} \boldsymbol{\Lambda}_{\text{pos}}^{\beta_k} \right) \mathbf{v}_{k-1} - \eta_k \boldsymbol{\Lambda}_{\text{pos}}^{\beta_k} \boldsymbol{\theta}_{k-1} + \eta_k \boldsymbol{\Lambda}_{\text{pos}}^{\beta_k} \boldsymbol{\mu}_{\text{pos}}^{\beta_k}, \end{aligned} \quad (65)$$

and for the updated position, we have

$$\begin{aligned} \boldsymbol{\theta}_k &= \boldsymbol{\theta}_{k-\frac{1}{2}} + \frac{\eta_k}{2} \hat{\mathbf{v}}_k \\ &= \boldsymbol{\theta}_{k-1} + \frac{\eta_k}{2} \mathbf{v}_{k-1} + \frac{\eta_k}{2} \left( \left( \mathbf{I} - \frac{\eta_k^2}{2} \boldsymbol{\Lambda}_{\text{pos}}^{\beta_k} \right) \mathbf{v}_{k-1} - \eta_k \boldsymbol{\Lambda}_{\text{pos}}^{\beta_k} \boldsymbol{\theta}_{k-1} + \eta_k \boldsymbol{\Lambda}_{\text{pos}}^{\beta_k} \boldsymbol{\mu}_{\text{pos}}^{\beta_k} \right) \\ &= \left( \mathbf{I} - \frac{\eta_k^2}{2} \boldsymbol{\Lambda}_{\text{pos}}^{\beta_k} \right) \boldsymbol{\theta}_{k-1} + \left( \eta_k \mathbf{I} - \frac{\eta_k^3}{4} \boldsymbol{\Lambda}_{\text{pos}}^{\beta_k} \right) \mathbf{v}_{k-1} + \frac{\eta_k^2}{2} \boldsymbol{\Lambda}_{\text{pos}}^{\beta_k} \boldsymbol{\mu}_{\text{pos}}^{\beta_k}. \end{aligned} \quad (66)$$

## B.2 Expected DAIS for Bayesian Linear Regression

In this section, we derive the gap between the exact log marginal likelihood and the lower bound given in expectation by DAIS.

If  $\mathbf{y}$  is distributed as a Gaussian with mean  $\mathbf{X}\boldsymbol{\theta}$  and covariance  $\sigma^2\mathbf{I}$ , and  $q(\boldsymbol{\theta})$  is the density of a random variable with mean  $\boldsymbol{\mu}_q$  and covariance  $\boldsymbol{\Sigma}_q$ , then the expected log-likelihood is

$$\begin{aligned}
\mathbb{E}_q [\log p(\mathbf{y}|\mathbf{X}, \boldsymbol{\theta})] &= \mathbb{E}_q \left[ -\frac{n}{2} \log(2\pi\sigma^2) - \frac{1}{2\sigma^2} (\mathbf{y} - \mathbf{X}\boldsymbol{\theta})^\top (\mathbf{y} - \mathbf{X}\boldsymbol{\theta}) \right] \\
&= \mathbb{E}_q \left[ -\frac{n}{2} \log(2\pi\sigma^2) - \frac{1}{2\sigma^2} (\mathbf{y}^\top \mathbf{y} - 2\boldsymbol{\theta}^\top \mathbf{X}^\top \mathbf{y} + \boldsymbol{\theta}^\top \mathbf{X}^\top \mathbf{X} \boldsymbol{\theta}) \right] \\
&= -\frac{n}{2} \log(2\pi\sigma^2) - \frac{1}{2\sigma^2} (\mathbf{y}^\top \mathbf{y} - 2\boldsymbol{\mu}_q^\top \mathbf{X}^\top \mathbf{y} + \text{Tr}(\mathbf{X}^\top \mathbf{X} \boldsymbol{\Sigma}_q) + \boldsymbol{\mu}_q^\top \mathbf{X}^\top \mathbf{X} \boldsymbol{\mu}_q) \\
&= -\frac{n}{2} \log(2\pi\sigma^2) - \frac{1}{2\sigma^2} (\mathbf{y} - \mathbf{X}\boldsymbol{\mu}_q)^\top (\mathbf{y} - \mathbf{X}\boldsymbol{\mu}_q) - \frac{1}{2} \text{Tr}(\boldsymbol{\Lambda}_{\text{lld}} \boldsymbol{\Sigma}_q).
\end{aligned} \tag{67}$$

If  $p(\boldsymbol{\theta})$  is the density of a Gaussian with mean  $\boldsymbol{\mu}_p$  and covariance  $\boldsymbol{\Sigma}_p$ , and if  $q(\boldsymbol{\theta})$  is the density of another random variable with mean  $\boldsymbol{\mu}_q$  and covariance  $\boldsymbol{\Sigma}_q$ , then

$$\begin{aligned}
\mathbb{E}_q [\log p(\boldsymbol{\theta})] &= \mathbb{E}_q \left[ -\frac{d}{2} \log(2\pi) - \frac{1}{2} \log |\boldsymbol{\Sigma}_p| - \frac{1}{2} (\boldsymbol{\theta} - \boldsymbol{\mu}_p)^\top \boldsymbol{\Lambda}_p (\boldsymbol{\theta} - \boldsymbol{\mu}_p) \right] \\
&= \mathbb{E}_q \left[ -\frac{d}{2} \log(2\pi) - \frac{1}{2} \log |\boldsymbol{\Sigma}_p| - \frac{1}{2} (\boldsymbol{\theta}^\top \boldsymbol{\Lambda}_p \boldsymbol{\theta} - 2\boldsymbol{\mu}_p^\top \boldsymbol{\Lambda}_p \boldsymbol{\theta} + \boldsymbol{\mu}_p^\top \boldsymbol{\Lambda}_p \boldsymbol{\mu}_p) \right] \\
&= -\frac{d}{2} \log(2\pi) - \frac{1}{2} \log |\boldsymbol{\Sigma}_p| - \frac{1}{2} (\text{Tr}(\boldsymbol{\Lambda}_p \boldsymbol{\Sigma}_q) + \boldsymbol{\mu}_q^\top \boldsymbol{\Lambda}_p \boldsymbol{\mu}_q - 2\boldsymbol{\mu}_p^\top \boldsymbol{\Lambda}_p \boldsymbol{\mu}_q + \boldsymbol{\mu}_p^\top \boldsymbol{\Lambda}_p \boldsymbol{\mu}_p) \\
&= -\frac{d}{2} \log(2\pi) - \frac{1}{2} \log |\boldsymbol{\Sigma}_p| - \frac{1}{2} \text{Tr}(\boldsymbol{\Lambda}_p \boldsymbol{\Sigma}_q) - \frac{1}{2} (\boldsymbol{\mu}_q - \boldsymbol{\mu}_p)^\top \boldsymbol{\Lambda}_p (\boldsymbol{\mu}_q - \boldsymbol{\mu}_p).
\end{aligned} \tag{68}$$

Given the above results, we now compute the DAIS lower bound:

$$\begin{aligned}
\mathcal{L}_{\text{DAIS}} &= \mathbb{E}_{q_{\text{fwd}}} \left[ \log f_K(\boldsymbol{\theta}_K) - \log p_0(\boldsymbol{\theta}_0) + \sum_{k=1}^K \log \frac{\pi(\hat{\mathbf{v}}_k)}{\pi(\mathbf{v}_{k-1})} \right] \\
&= \mathbb{E}_{q_{\text{fwd}}} \left[ \log p(\mathcal{D}|\boldsymbol{\theta}_K) + \log p_0(\boldsymbol{\theta}_K) - \log p_0(\boldsymbol{\theta}_0) + \sum_{k=1}^K \log \frac{\pi(\hat{\mathbf{v}}_k)}{\pi(\mathbf{v}_{k-1})} \right] \\
&= \left( -\frac{n}{2} \log(2\pi\sigma^2) - \frac{1}{2\sigma^2} \mathbf{y}^\top \mathbf{y} + \frac{1}{\sigma^2} \boldsymbol{\mu}_K^\top \mathbf{X}^\top \mathbf{y} - \frac{1}{2} \text{Tr}(\boldsymbol{\Lambda}_{\text{lld}} \boldsymbol{\Sigma}_K) - \frac{1}{2} \boldsymbol{\mu}_K^\top \boldsymbol{\Lambda}_{\text{lld}} \boldsymbol{\mu}_K \right) \\
&\quad \left( -\frac{1}{2} \text{Tr}(\boldsymbol{\Lambda}_p \boldsymbol{\Sigma}_K) - \frac{1}{2} \boldsymbol{\mu}_K^\top \boldsymbol{\Lambda}_p \boldsymbol{\mu}_K + \boldsymbol{\mu}_p^\top \boldsymbol{\Lambda}_p \boldsymbol{\mu}_K - \frac{1}{2} \boldsymbol{\mu}_p^\top \boldsymbol{\Lambda}_p \boldsymbol{\mu}_p \right) + \frac{d}{2} + \mathbb{E}_{q_{\text{fwd}}} \left[ \sum_{k=1}^K \log \frac{\pi(\hat{\mathbf{v}}_k)}{\pi(\mathbf{v}_{k-1})} \right] \\
&= -\frac{n}{2} \log(2\pi\sigma^2) - \frac{1}{2\sigma^2} \mathbf{y}^\top \mathbf{y} + \frac{1}{\sigma^2} \boldsymbol{\mu}_K^\top \mathbf{X}^\top \mathbf{y} - \frac{1}{2} \text{Tr}(\boldsymbol{\Lambda}_{\text{pos}} \boldsymbol{\Sigma}_K) - \frac{1}{2} \boldsymbol{\mu}_K^\top \boldsymbol{\Lambda}_{\text{pos}} \boldsymbol{\mu}_K \\
&\quad + \boldsymbol{\mu}_p^\top \boldsymbol{\Lambda}_p \boldsymbol{\mu}_K - \frac{1}{2} \boldsymbol{\mu}_p^\top \boldsymbol{\Lambda}_p \boldsymbol{\mu}_p + \frac{d}{2} + \mathbb{E}_{q_{\text{fwd}}} \left[ \sum_{k=1}^K \log \frac{\pi(\hat{\mathbf{v}}_k)}{\pi(\mathbf{v}_{k-1})} \right]
\end{aligned} \tag{69}$$

For comparison, we compute the log marginal likelihood by completing the square and recognizing the normalization of a Gaussian density:

$$\begin{aligned}
\log p(\mathcal{D}) &= \log \int p(\mathcal{D}|\boldsymbol{\theta})p_0(\boldsymbol{\theta})d\boldsymbol{\theta} \\
&= \log \int (2\pi\sigma^2)^{-n/2} \exp\left(-\frac{1}{2}(\boldsymbol{\theta} - \boldsymbol{\mu}_*)^\top \boldsymbol{\Lambda}_{\text{lld}}(\boldsymbol{\theta} - \boldsymbol{\mu}_*) + \frac{1}{2}\boldsymbol{\mu}_*^\top \boldsymbol{\Lambda}_{\text{lld}}\boldsymbol{\mu}_* - \frac{1}{2\sigma^2}\mathbf{y}^\top \mathbf{y}\right) \\
&\quad (2\pi)^{-d/2}|\boldsymbol{\Sigma}_p|^{-1/2} \exp\left(-\frac{1}{2}(\boldsymbol{\theta} - \boldsymbol{\mu}_p)^\top \boldsymbol{\Lambda}_p(\boldsymbol{\theta} - \boldsymbol{\mu}_p)\right) d\boldsymbol{\theta} \\
&= \log \int (2\pi\sigma^2)^{-n/2} (2\pi)^{-d/2}|\boldsymbol{\Sigma}_p|^{-1/2} \exp\left(-\frac{1}{2}(\boldsymbol{\theta} - \boldsymbol{\mu}_{\text{pos}})^\top \boldsymbol{\Lambda}_{\text{pos}}(\boldsymbol{\theta} - \boldsymbol{\mu}_{\text{pos}})\right. \\
&\quad \left. + \frac{1}{2}\boldsymbol{\mu}_{\text{pos}}^\top \boldsymbol{\Lambda}_{\text{pos}}\boldsymbol{\mu}_{\text{pos}} - \frac{1}{2\sigma^2}\mathbf{y}^\top \mathbf{y} - \frac{1}{2}\boldsymbol{\mu}_p^\top \boldsymbol{\Lambda}_p\boldsymbol{\mu}_p\right) d\boldsymbol{\theta} \\
&= -\frac{n}{2} \log(2\pi\sigma^2) - \frac{d}{2} \log(2\pi) - \frac{1}{2} \log|\boldsymbol{\Sigma}_p| + \frac{1}{2}\boldsymbol{\mu}_{\text{pos}}^\top \boldsymbol{\Lambda}_{\text{pos}}\boldsymbol{\mu}_{\text{pos}} - \frac{1}{2\sigma^2}\mathbf{y}^\top \mathbf{y} - \frac{1}{2}\boldsymbol{\mu}_p^\top \boldsymbol{\Lambda}_p\boldsymbol{\mu}_p \\
&\quad + \underbrace{\log \int \exp\left(-\frac{1}{2}(\boldsymbol{\theta} - \boldsymbol{\mu}_{\text{pos}})^\top \boldsymbol{\Lambda}_{\text{pos}}(\boldsymbol{\theta} - \boldsymbol{\mu}_{\text{pos}})\right) d\boldsymbol{\theta}}_{+\frac{d}{2}\log(2\pi) + \frac{1}{2}\log|\boldsymbol{\Sigma}_{\text{pos}}|} \\
&= -\frac{n}{2} \log(2\pi\sigma^2) + \frac{1}{2} \log \frac{|\boldsymbol{\Sigma}_{\text{pos}}|}{|\boldsymbol{\Sigma}_p|} + \frac{1}{2}\boldsymbol{\mu}_{\text{pos}}^\top \boldsymbol{\Lambda}_{\text{pos}}\boldsymbol{\mu}_{\text{pos}} - \frac{1}{2\sigma^2}\mathbf{y}^\top \mathbf{y} - \frac{1}{2}\boldsymbol{\mu}_p^\top \boldsymbol{\Lambda}_p\boldsymbol{\mu}_p
\end{aligned} \tag{70}$$

The gap is thus

$$\begin{aligned}
\log p(\mathcal{D}) - \mathcal{L}_{\text{DAIS}} &= -\frac{n}{2} \log(2\pi\sigma^2) + \frac{1}{2} \log \frac{|\boldsymbol{\Sigma}_{\text{pos}}|}{|\boldsymbol{\Sigma}_p|} + \frac{1}{2}\boldsymbol{\mu}_{\text{pos}}^\top \boldsymbol{\Lambda}_{\text{pos}}\boldsymbol{\mu}_{\text{pos}} - \frac{1}{2\sigma^2}\mathbf{y}^\top \mathbf{y} \\
&\quad - \frac{1}{2}\boldsymbol{\mu}_p^\top \boldsymbol{\Lambda}_p\boldsymbol{\mu}_p + \frac{n}{2} \log(2\pi\sigma^2) + \frac{1}{2\sigma^2}\mathbf{y}^\top \mathbf{y} - \frac{1}{\sigma^2}\boldsymbol{\mu}_K^\top \mathbf{X}^\top \mathbf{y} + \frac{1}{2} \text{Tr}(\boldsymbol{\Lambda}_{\text{pos}} \boldsymbol{\Sigma}_K) \\
&\quad + \frac{1}{2}\boldsymbol{\mu}_K^\top \boldsymbol{\Lambda}_{\text{pos}}\boldsymbol{\mu}_K - \boldsymbol{\mu}_p^\top \boldsymbol{\Lambda}_p\boldsymbol{\mu}_K + \frac{1}{2}\boldsymbol{\mu}_p^\top \boldsymbol{\Lambda}_p\boldsymbol{\mu}_p - \frac{d}{2} - \mathbb{E}_{q_{\text{fwd}}} \left[ \sum_{k=1}^K \log \frac{\pi(\hat{\mathbf{v}}_k)}{\pi(\mathbf{v}_{k-1})} \right] \\
&= \underbrace{\frac{1}{2}\boldsymbol{\mu}_K^\top \boldsymbol{\Lambda}_{\text{pos}}\boldsymbol{\mu}_K - \frac{1}{\sigma^2}\boldsymbol{\mu}_K^\top \mathbf{X}^\top \mathbf{y} - \boldsymbol{\mu}_p^\top \boldsymbol{\Lambda}_p\boldsymbol{\mu}_K + \frac{1}{2}\boldsymbol{\mu}_{\text{pos}}^\top \boldsymbol{\Lambda}_{\text{pos}}\boldsymbol{\mu}_{\text{pos}}}_{\frac{1}{2}\|\boldsymbol{\mu}_K - \boldsymbol{\mu}_{\text{pos}}\|_{\boldsymbol{\Lambda}_{\text{pos}}}^2} \\
&\quad + \frac{1}{2} \text{Tr}(\boldsymbol{\Lambda}_{\text{pos}} \boldsymbol{\Sigma}_K) - \frac{d}{2} + \frac{1}{2} \log \frac{|\boldsymbol{\Sigma}_{\text{pos}}|}{|\boldsymbol{\Sigma}_p|} - \mathbb{E}_{q_{\text{fwd}}} \left[ \sum_{k=1}^K \log \frac{\pi(\hat{\mathbf{v}}_k)}{\pi(\mathbf{v}_{k-1})} \right]
\end{aligned} \tag{71}$$

### B.3 DAIS Update under Full Momentum Refreshment

The following quantities are used in our convergence analysis for DAIS, which assumes full momentum refreshment, i.e. that  $\gamma = 0$ .

For the mean of the updated position, we have

$$\begin{aligned}
\boldsymbol{\mu}_k &= \mathbb{E}_{q_{\text{fwd}}} \left[ \left( \mathbf{I} - \frac{\eta_k^2}{2} \boldsymbol{\Lambda}_{\text{pos}}^{\beta_k} \right) \boldsymbol{\theta}_{k-1} + \left( \eta_k \mathbf{I} - \frac{\eta_k^3}{4} \boldsymbol{\Lambda}_{\text{pos}}^{\beta_k} \right) \mathbf{v}_{k-1} + \frac{\eta_k^2}{2} \boldsymbol{\Lambda}_{\text{pos}}^{\beta_k} \boldsymbol{\mu}_{\text{pos}}^{\beta_k} \right] \\
&= \left( \mathbf{I} - \frac{\eta_k^2}{2} \boldsymbol{\Lambda}_{\text{pos}}^{\beta_k} \right) \boldsymbol{\mu}_{k-1} + \frac{\eta_k^2}{2} \boldsymbol{\Lambda}_{\text{pos}}^{\beta_k} \boldsymbol{\mu}_{\text{pos}}^{\beta_k}
\end{aligned} \tag{72}$$

as  $\mathbb{E}_{q_{\text{fwd}}}[\mathbf{v}_{k-1}] = \mathbf{0}$  under full momentum refreshment.

For the covariance of the updated position, we have

$$\boldsymbol{\theta}_k - \boldsymbol{\mu}_k = \left( \mathbf{I} - \frac{\eta_k^2}{2} \boldsymbol{\Lambda}_{\text{pos}}^{\beta_k} \right) (\boldsymbol{\theta}_{k-1} - \boldsymbol{\mu}_{k-1}) + \left( \eta_k \mathbf{I} - \frac{\eta_k^3}{4} \boldsymbol{\Lambda}_{\text{pos}}^{\beta_k} \right) \mathbf{v}_{k-1} \tag{73}$$

and so

$$\begin{aligned}
\boldsymbol{\Sigma}_k &= \mathbb{E}_{q_{\text{fwd}}} [(\boldsymbol{\theta}_k - \boldsymbol{\mu}_k)(\boldsymbol{\theta}_k - \boldsymbol{\mu}_k)^\top] \\
&= \left( \mathbf{I} - \frac{\eta^2}{2} \boldsymbol{\Lambda}_{\text{pos}}^{\beta_k} \right) \boldsymbol{\Sigma}_{k-1} \left( \mathbf{I} - \frac{\eta^2}{2} \boldsymbol{\Lambda}_{\text{pos}}^{\beta_k} \right)^\top + \left( \eta \mathbf{I} - \frac{\eta^3}{4} \boldsymbol{\Lambda}_{\text{pos}}^{\beta_k} \right) \mathbb{E}[\mathbf{v}_{k-1} \mathbf{v}_{k-1}^\top] \left( \eta \mathbf{I} - \frac{\eta^3}{4} \boldsymbol{\Lambda}_{\text{pos}}^{\beta_k} \right)^\top \\
&= \left( \mathbf{I} - \frac{\eta^2}{2} \boldsymbol{\Lambda}_{\text{pos}}^{\beta_k} \right) \boldsymbol{\Sigma}_{k-1} \left( \mathbf{I} - \frac{\eta^2}{2} \boldsymbol{\Lambda}_{\text{pos}}^{\beta_k} \right)^\top + \eta^2 \mathbf{I} - \frac{\eta^4}{4} \boldsymbol{\Lambda}_{\text{pos}}^{\beta_k} - \frac{\eta^4}{4} \boldsymbol{\Lambda}_{\text{pos}}^{\beta_k} + \frac{\eta^6}{16} (\boldsymbol{\Lambda}_{\text{pos}}^{\beta_k})^2 \\
&= \left( \mathbf{I} - \frac{\eta^2}{2} \boldsymbol{\Lambda}_{\text{pos}}^{\beta_k} \right) (\boldsymbol{\Sigma}_{k-1} - \boldsymbol{\Sigma}_{\text{pos}}^{\beta_k}) \left( \mathbf{I} - \frac{\eta^2}{2} \boldsymbol{\Lambda}_{\text{pos}}^{\beta_k} \right)^\top + \boldsymbol{\Sigma}_{\text{pos}}^{\beta_k} - \frac{\eta^4}{4} \boldsymbol{\Lambda}_{\text{pos}}^{\beta_k} + \frac{\eta^6}{16} (\boldsymbol{\Lambda}_{\text{pos}}^{\beta_k})^2
\end{aligned} \tag{74}$$

where we leverage the fact that  $\boldsymbol{\mu}_{k-1}$  and  $\mathbf{v}_{k-1}$  are independent and hence uncorrelated under full momentum refreshment, and that  $\mathbf{v}_{k-1} \sim \mathcal{N}(\mathbf{0}, \mathbf{I})$  so  $\mathbb{E}[\mathbf{v}_{k-1} \mathbf{v}_{k-1}^\top] = \mathbf{I}$ .

For the mean of the updated momentum, we have

$$\boldsymbol{\mu}_k^{\mathbf{v}} = \mathbb{E}_{q_{\text{fwd}}} \left[ \left( \mathbf{I} - \frac{\eta_k^2}{2} \boldsymbol{\Lambda}_{\text{pos}}^{\beta_k} \right) \mathbf{v}_{k-1} - \eta_k \boldsymbol{\Lambda}_{\text{pos}}^{\beta_k} \boldsymbol{\theta}_{k-1} + \eta_k \boldsymbol{\Lambda}_{\text{pos}}^{\beta_k} \boldsymbol{\mu}_{\text{pos}}^{\beta_k} \right] = \eta_k \boldsymbol{\Lambda}_{\text{pos}}^{\beta_k} (\boldsymbol{\mu}_{\text{pos}}^{\beta_k} - \boldsymbol{\mu}_{k-1}) \tag{75}$$

where we again use  $\mathbb{E}_{q_{\text{fwd}}} [\mathbf{v}_{k-1}] = \mathbf{0}$ .

For the covariance of the updated momentum, we have

$$\begin{aligned}
\boldsymbol{\Sigma}_k^{\mathbf{v}} &= \mathbb{E}_{q_{\text{fwd}}} [(\hat{\mathbf{v}}_k - \boldsymbol{\mu}_k^{\mathbf{v}})(\hat{\mathbf{v}}_k - \boldsymbol{\mu}_k^{\mathbf{v}})^\top] \\
&= \left( \mathbf{I} - \frac{\eta_k^2}{2} \boldsymbol{\Lambda}_{\text{pos}}^{\beta_k} \right) \mathbb{E}_{q_{\text{fwd}}} [\mathbf{v}_{k-1} \mathbf{v}_{k-1}^\top] \left( \mathbf{I} - \frac{\eta_k^2}{2} \boldsymbol{\Lambda}_{\text{pos}}^{\beta_k} \right)^\top + \eta_k^2 \boldsymbol{\Lambda}_{\text{pos}}^{\beta_k} \boldsymbol{\Sigma}_{k-1} \boldsymbol{\Lambda}_{\text{pos}}^{\beta_k} \\
&= \left( \mathbf{I} - \frac{\eta_k^2}{2} \boldsymbol{\Lambda}_{\text{pos}}^{\beta_k} \right)^2 + \eta_k^2 \boldsymbol{\Lambda}_{\text{pos}}^{\beta_k} \boldsymbol{\Sigma}_{k-1} \boldsymbol{\Lambda}_{\text{pos}}^{\beta_k}
\end{aligned} \tag{76}$$

where we again leverage the independence of  $\mathbf{v}_{k-1}$  and  $\boldsymbol{\theta}_k$ , and  $\mathbb{E}[\mathbf{v}_{k-1} \mathbf{v}_{k-1}^\top] = \mathbf{I}$ .

#### B.4 Noisy Model for Bayesian Linear Regression

In this section, we justify the additive noise model we used in analyzing the stochastic version of DAIS. In particular, the mini-batch gradient has the following form:

$$\tilde{\nabla}_{\boldsymbol{\theta}} \log f_{\beta_k}(\boldsymbol{\theta}) = -\boldsymbol{\Lambda}_p(\boldsymbol{\theta} - \boldsymbol{\mu}_p) + \frac{\beta_k n}{\sigma^2} \mathbf{x} (y - \mathbf{x}^\top \boldsymbol{\theta}), \tag{77}$$

where  $(\mathbf{x}, y)$  is one training sample and  $n$  is the number of training samples in the dataset. Compared to the full-batch gradient in (60), we have

$$\tilde{\nabla}_{\boldsymbol{\theta}} \log f_{\beta_k}(\boldsymbol{\theta}) - \nabla_{\boldsymbol{\theta}} \log f_{\beta_k}(\boldsymbol{\theta}) = \frac{\beta_k}{\sigma^2} (n \mathbf{x} \mathbf{x}^\top - \mathbf{X}^\top \mathbf{X}) \boldsymbol{\theta} + \frac{\beta_k}{\sigma^2} (n \mathbf{x} y - \mathbf{X}^\top \mathbf{y}) \tag{78}$$

As long as the problem is not linearly solvable, i.e.,  $\mathbf{y} = \mathbf{X} \boldsymbol{\mu}^* + \boldsymbol{\varepsilon}$ , we have

$$\tilde{\nabla}_{\boldsymbol{\theta}} \log f_{\beta_k}(\boldsymbol{\theta}) - \nabla_{\boldsymbol{\theta}} \log f_{\beta_k}(\boldsymbol{\theta}) = \frac{\beta_k}{\sigma^2} (n \mathbf{x} \mathbf{x}^\top - \mathbf{X}^\top \mathbf{X}) (\boldsymbol{\theta} - \boldsymbol{\mu}_*) + \frac{\beta_k}{\sigma^2} (n \mathbf{x} \boldsymbol{\varepsilon} - \mathbf{X}^\top \boldsymbol{\varepsilon}) \tag{79}$$

We typically refer to the first term in (79) as multiplicative noise as it depends on  $\boldsymbol{\theta} - \boldsymbol{\mu}_*$  and the second term as additive noise.

## C Implementation Details and Additional Results

### C.1 Implementation Details for Training Experiments

The prior  $p(\mathbf{z})$  is a 50-dimensional standard Gaussian distribution. The conditional distributions  $p(\mathbf{x}_i | \mathbf{z})$  are independent Bernoulli, with the decoder parameterized by two hidden layers, each with 200 tanh units. The variational posterior  $q(\mathbf{z} | \mathbf{x})$  is also a 50-dimensional Gaussian distribution with diagonal covariance, whose mean and variance are both parameterized by two hidden layers with

200 tanh units. For training, we used Adam [Kingma and Ba, 2015] optimizer for 1,500 epochs with initial learning rate 0.001 and we decay the learning rate by factor 0.8 every 100 epochs. By default, we use constant step size and partial momentum refreshment  $\gamma = 0.9$  for all iterations. For each setting, we tune step-size  $\eta$  by grid search with the search range  $\{0.02, 0.04, 0.06, 0.08, 0.10\}$ .

For DAIS (adapt), we learn the annealing scheme along with VAE parameters. In particular, the annealing scheme is parameterized as  $\beta_k = \sum_{i=1}^k p_i$  with  $p = \text{softmax}(z)$  where  $z \in \mathbb{R}^K$  is the trainable parameters. Using this parameterization, we guarantee that  $\beta_i \geq 0$ ,  $\beta_K = 1$  and  $\beta_{i+1} \geq \beta_i$ . To avoid collapse, we add a small amount of entropy regularization on  $p$  with a coefficient of 0.01. With a stronger entropy regularizer, the learned annealing scheme would be closer to linear scheme  $\beta_k = \frac{k}{K}$ . We note that the performance is insensitive to the entropy regularization coefficient.

## C.2 Implementation Details for Evaluation Experiments

For AIS, we run 10 leapfrog steps (followed by MH accept-reject steps) for every intermediate distribution to be consistent with Wu et al. [2016]. By default, we use linear annealing scheme with  $\beta_k = \frac{k}{K}$ . For HAIS and DAIS, we use constant step-size and partial momentum refreshment with  $\gamma = 0.9$  for simulations. Importantly, we only tune the step-size for  $K = 10$  and then we employ the optimal scaling scheme we derived in Theorem 1 with  $c = \frac{1}{4}$ . By grid search, we find  $\eta = 0.08$  is good overall for all the models with  $K = 10$ , so we use the step-size  $\eta$  defined as  $0.08 \times (K/10)^{-0.25}$  for any run with  $K$  intermediate distributions. For AIS, its step-size is adapted throughout the course of training with a target accept rate of 0.65 in the MH step. We increase the step-size by multiplying 1.02 when the accept rate is larger than 0.65, otherwise we multiply it with factor 0.98. For all curves, we average over 10 runs.

## C.3 Additional Results for Evaluation

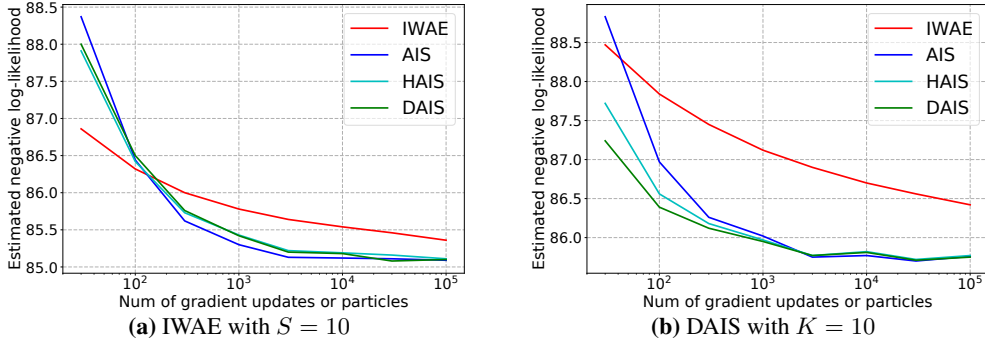


Figure 3: Results of different algorithms in evaluating IWAE- or DAIS-trained models.

## D Notes on Memory-Efficient DAIS

---

### Algorithm 2 Reversible DAIS (forward)

---

**Require:** seed  $s_0$ , initial state  $\theta_0 \sim p_0(\theta)$ ,  $\mathbf{v}_0 \sim \pi \triangleq \mathcal{N}(\mathbf{0}, \mathbf{M})$

**for**  $k = 1, \dots, K$  **do**

$\theta_{k-\frac{1}{2}} \leftarrow \theta_{k-1} + \frac{\eta_k}{2} \mathbf{M}^{-1} \mathbf{v}_{k-1}$

$\hat{\mathbf{v}}_k \leftarrow \mathbf{v}_{k-1} + \eta_k \nabla \log f_{\beta_k}(\theta_{k-\frac{1}{2}})$

$\theta_k \leftarrow \theta_{k-\frac{1}{2}} + \frac{\eta_k}{2} \mathbf{M}^{-1} \hat{\mathbf{v}}_k$

$s_k \leftarrow \text{FORWARD\_SEED}(s_{k-1})$

$\boldsymbol{\varepsilon}_k \sim \mathcal{N}(\mathbf{0}, \mathbf{M}; s_k)$

$\mathbf{v}_k \leftarrow \gamma \hat{\mathbf{v}}_k + \sqrt{1 - \gamma^2} \boldsymbol{\varepsilon}_k$

**end for**

**return**  $\theta_K, \mathbf{v}_K, s_K$

---

---

**Algorithm 3** Reversible DAIS (backward)

---

**Require:**  $s_K, \boldsymbol{\theta}_K, \mathbf{v}_K$   
**for**  $k = K, \dots, 1$  **do**  
     $\boldsymbol{\varepsilon}_k \sim \mathcal{N}(\mathbf{0}, \mathbf{M}; s_k)$   
     $\hat{\mathbf{v}}_k \leftarrow \frac{1}{\gamma_k} \left( \mathbf{v}_k - \sqrt{1 - \gamma^2} \boldsymbol{\varepsilon}_k \right)$   
     $s_{k-1} \leftarrow \text{BACKWARD\_SEED}(s_k)$   
     $\boldsymbol{\theta}_{k-\frac{1}{2}} \leftarrow \boldsymbol{\theta}_k - \frac{\eta_k}{2} \mathbf{M}^{-1} \hat{\mathbf{v}}_k$   
     $\mathbf{v}_{k-1} \leftarrow \hat{\mathbf{v}}_k - \eta_k \nabla \log f_{\beta_k}(\boldsymbol{\theta}_{k-\frac{1}{2}})$   
     $\boldsymbol{\theta}_{k-1} \leftarrow \boldsymbol{\theta}_{k-\frac{1}{2}} - \frac{\eta_k}{2} \mathbf{M}^{-1} \mathbf{v}_{k-1}$   
**end for**  
**return**  $\boldsymbol{\theta}_0, \mathbf{v}_0, s_0$

---

Algorithms 2 and 3 detail the simulation of DAIS dynamics in a reversible manner. The momentum refreshment step requires the reversible computation of a seed in order to retrieve noise samples. Reversibility is sufficient to facilitate reverse-mode differentiation through the chain without explicitly storing the DAIS trajectory. Hence, DAIS can be made memory-efficient while retaining differentiability to any of its parameters.

However, as detailed by [Maclaurin et al. \[2015\]](#), the division by  $\gamma_k$  for the computation of  $\hat{\mathbf{v}}_k$  in the backward simulation is problematic for finite-precision computation as information is lost with each step. This is combated with Algorithm 3 [[Maclaurin et al., 2015](#)] at the minute cost of  $\log_2(1/\gamma)$  bits per parameter per step.